Cosmological SPH simulations: A hybrid multi-phase model for star formation

Volker Springel[1]* and Lars Hernquist[2]‡

[1] *Max-Planck-Institut für Astrophysik, Karl-Schwarzschild-Straße 1, 85740 Garching bei München, Germany*
[2] *Harvard-Smithsonian Center for Astrophysics, 60 Garden Street, Cambridge, MA 02138, USA*

22 June 2002

ABSTRACT

We present a model for star formation and supernova feedback that describes the multi-phase structure of star forming gas on scales that are typically not resolved in cosmological simulations. Our approach includes radiative heating and cooling, the growth of cold clouds embedded in an ambient hot medium, star formation in these clouds, feedback from supernovae in the form of thermal heating and cloud evaporation, galactic winds and outflows, and metal enrichment. Implemented using smoothed particle hydrodynamics (SPH), our scheme is a significantly modified and extended version of the grid-based method of Yepes et al. (1997), and enables us to achieve high dynamic range in simulations of structure formation.

We discuss properties of the feedback model in detail and show that it predicts a self-regulated, quiescent mode of star formation, which, in particular, stabilises the star forming gaseous layers of disk galaxies. The parameterisation of this mode can be reduced to a single free quantity which determines the overall timescale for star formation. We fix this parameter numerically to match the observed rates of star formation in local disk galaxies. When normalised in this manner, cosmological simulations employing our model nevertheless overproduce the observed cosmic abundance of stellar material. We are thus motivated to extend our feedback model to include galactic winds associated with star formation.

Using small-scale simulations of individual star-forming disk galaxies, we show that these winds produce either galactic fountains or outflows, depending on the depth of the gravitational potential. In low-mass haloes, winds can greatly suppress the overall efficiency of star formation. When incorporated into cosmological simulations, our combined model for star formation and winds predicts a cosmic star formation density that is consistent with observations, provided that the winds are sufficiently energetic. Moreover, outflows from galaxies in these simulations drive chemical enrichment of the intergalactic medium, in principle accounting for the presence of metals in the Lyman alpha forest.

Key words: galaxies: evolution – galaxies: formation – methods: numerical.

1 INTRODUCTION

The past two decades have witnessed the emergence of a successful class of theoretical models to explain the formation of structure in the Universe. In these "hierarchical" scenarios, cold dark matter (CDM) forms the dominant mass component, and structure grows via gravitational instability from primordial perturbations seeded by inflation. Galaxy formation proceeds "bottom-up" in this picture, with smaller galaxies forming first, and larger objects being assembled through merging of less massive building blocks.

Numerical simulations have become an important tool for exploring the detailed predictions of these models. For example, the clustering properties of matter on large scales, where gasdynamical forces are negligible compared to gravity, can now be computed with high precision. However, extending these studies to understand the formation of luminous components of galaxies is considerably more difficult. Cosmological simulations that attempt to include the

---

* E-mail: volker@mpa-garching.mpg.de
‡ E-mail: lars@cfa.harvard.edu

essential physical processes associated with galaxy formation, namely radiative cooling and star formation, invariably encounter formidable difficulties. For this reason, the most popular approach to date for describing hierarchical galaxy formation has been the so-called "semi-analytic" technique (e.g. White & Frenk, 1991; Lacey & Silk, 1991; Kauffmann et al., 1993, 1994; Cole et al., 1994), in which highly simplified prescriptions for the baryonic physics are combined with Monte-Carlo methods to construct merging history trees. In recent times, these Monte-Carlo trees have been replaced with merging histories obtained directly from high-resolution N-body simulations (Kauffmann et al., 1999a,b; Springel et al., 2001a).

Some impressive successes in direct numerical simulation of cosmological hydrodynamics have been obtained since this method was pioneered more than a decade ago (Evrard, 1988, 1990; Hernquist, 1989; Hernquist & Katz, 1989; Navarro & Benz, 1991; Barnes & Hernquist, 1991; Katz & Gunn, 1991; Hiotelis & Voglis, 1991; Thomas & Couchman, 1992; Katz et al., 1992; Cen & Ostriker, 1993). For example, these studies improved our understanding of quasar absorption line systems (e.g. Cen et al., 1994; Zhang et al., 1995; Hernquist et al., 1996), the intergalactic medium (e.g. Cen & Ostriker, 1993, 2000; Katz et al., 1996, 1999; Weinberg et al., 1997, 2002; Steinmetz & Müller, 1995; Bryan et al., 1994; Bryan & Norman, 1998; Blanton et al., 1999; Pearce et al., 1999, 2001), and galaxy formation (e.g. Katz & Gunn, 1991; Navarro & White, 1994a; Steinmetz & Müller, 1995; Mihos & Hernquist, 1996; Walker et al., 1996; Navarro & Steinmetz, 1997; Steinmetz & Navarro, 1999).

However, the numerical modelling of key processes related to star formation and associated feedback by supernovae and stellar winds has remained problematic. Because radiative cooling is particularly efficient in dense, low-mass haloes at high redshift, simulations are confronted with an overcooling problem, which is typically manifested through an overproduction of stars. Semi-analytic treatments indicate that a physical handling of feedback processes is required to regulate star formation and reduce the fraction of baryons that collapse in the centres of haloes. Unfortunately, it is not clear how best to incorporate feedback processes into simulations of galaxy formation, although they appear to be crucially important to a successful description of hierarchical CDM universes.

Here, we present a model for star formation and feedback that goes beyond a purely phenomenological description. In most attempts to simulate galaxy formation, the gas within galaxies is treated as a single phase medium and is converted into stars on some characteristic timescale, which is usually related to the local dynamical time. Often, auxiliary criteria requiring that the flow be locally converging or Jeans unstable are also invoked to restrict the eligibility of gas fluid elements for star formation. Based on an assumed stellar initial mass function (IMF), it is then straightforward to work out the expected rate of energy input due to associated supernovae. However, it is not clear how this "feedback energy" should be deposited into the gas. Simply augmenting the thermal reservoir of the gas has little effect, because the cooling time in the dense single-phase medium in these simulations is so short that the energy is promptly radiated away. Consequently, pure thermal feedback in this manner fails to solve the overcooling problem.

Other approaches have been attempted to prevent this rapid loss of feedback energy, thereby providing a back-reaction on star formation (see Kay et al., 2002, for a recent comparison of the most common of these methods). For example, Thacker & Couchman (2000) temporarily lower the densities of SPH particles receiving feedback energy to prevent immediate energy loss. Alternatively, such particles have been treated adiabatically for a brief period of time after acquiring feedback energy (Gerritsen & Icke, 1997). Although crude, these methods show some success in regulating star formation. For example, Thacker & Couchman (2001) have recently found that the angular momentum problem in the formation of disk galaxies can be alleviated through the combined effects of a smoothed deposition of feedback energy with a delay of cooling by 30 Myr.

Another method for depositing the energy is through kinetic feedback, where radial momentum kicks are imparted to particles surrounding sites of star formation (e.g. Navarro & White, 1993; Mihos & Hernquist, 1994), but the fraction of feedback energy that must be put into this channel depends on numerical details of the simulations. Also, the size of the affected regions depends on spatial resolution, and is in general much larger than the physical scale of individual supernova remnants.

Sommer-Larsen et al. (1999) experimented with yet more extreme versions of feedback in order to investigate the effects of galactic outflows. For example, in their "blow-out" simulations, they identified all dense, cold gas at $z = 2.4$ and instantly removed it and redistributed it uniformly in spherical shells around the centres of the gas clumps. While this is clearly a highly artificial model, it demonstrated that outflows can have a large impact on galaxy formation. In particular, the loss of angular momentum by the gaseous component was greatly reduced in their simulations, alleviating the apparent discrepancy between observed and simulated values of the specific angular momentum of galactic disks. Scannapieco et al. (2001) used a similar gas-removal technique to model galactic winds at high redshift.

A disadvantage common to many of these recipes is their explicit or implicit dependence on numerical details of the simulations. For example, if a criterion for star formation explicitly involves the mass of a particle, it is unclear in what sense numerical convergence for the star formation rate of a specific object can be expected if the simulation is repeated with a different mass resolution. Instead, the free parameters describing star formation may need to be recalibrated whenever the properties of the simulation are altered. Springel (2000) tried to overcome this problem by developing a feedback method based on an effective model for the star-forming interstellar medium (ISM), where turbulent motions on unresolved scales were postulated in an ad-hoc fashion to provide pressure support for the gas, thereby regulating star formation. In essence, feedback energy was only slowly thermalised in this method, thereby delaying the dissipation of feedback energy in a similar way to some of the models noted above.

Because the Lagrangian nature of smoothed particle hydrodynamics makes it relatively easy to obtain the high spatial dynamic range needed for simulations of galaxy formation, it has so far been the most popular numerical technique for studying this problem. However, star formation and feedback have also been incorporated into hydrodynamical mesh

codes (e.g. Cen & Ostriker, 1993; Gnedin, 1998), but their limited spatial resolution is a serious concern, because star formation occurs at substantially higher overdensities than can be resolved with a fixed grid in cosmological volumes. This is quite different when high-resolution Eulerian codes are applied to simulations of isolated galaxies, as in the work of Mac Low & Ferrara (1999), who carried out detailed studies of starbursts in dwarf galaxies. Eulerian codes have also been employed to directly resolve the multi-phase structure of the ISM, yet state-of-the-art simulations are either restricted to two dimensions (Wada & Norman, 1999), or can presently only resolve regions of size ∼100 pc or so in three dimensions (Wada, 2001).

Yepes et al. (1997) adopted an intermediate approach by developing a sub-grid model of a two-phase ISM and implementing it in an Eulerian code. Their spatial resolution was consequently relatively poor, despite restricting themselves to rather small cosmological volumes, but together with subsequent work (Elizondo et al., 1999a,b; Ascasibar et al., 2002) they were able to demonstrate a number of interesting properties of this scheme, which is physically better motivated than most of the models currently employed in cosmological SPH simulations. Because of this, we will base our analysis in part on their approach and on a first implementation of it in SPH by Hultman & Pharasyn (1999), yet we will significantly extend and modify the model. Our specific aim is to formulate a description of feedback which is physically motivated, numerically well specified, and suitable for simulating galaxy formation within large cosmological volumes. In what follows, we show that our model leads to self-regulation of star formation, and describe how it can be normalised by analysing its properties. Under the assumption that the normalisation obtained from observations of disk galaxies in the present Universe holds at all redshifts, we find that the resulting cosmic star history leads to an overprediction of the luminosity density of the universe. We then argue that galactic winds are a plausible mechanism for eliminating this discrepancy, and they simultaneously help to account for other observational data, like the metals found in the low-density intergalactic medium (IGM), and describe a phenomenological strategy for including these winds in cosmological simulations.

This paper is organised as follows. In Section 2, we summarise our new hybrid multi-phase model for quiescent star formation in detail, and analyse some of its basic properties. In Section 3, we discuss physical and observational constraints on the values of the model parameters. In Section 4, we extend the model by including galactic winds. We then describe our numerical implementation of the method in a parallel TreeSPH code for cosmic structure formation in Section 5. We present numerical results for the formation of disk galaxies in isolation, and for small simulations of cosmic structure formation in Section 6. Finally, we give conclusions in Section 7.

2 A MULTI-PHASE MODEL FOR QUIESCENT STAR FORMATION

We term our treatment of star formation and feedback a "hybrid" method because it does not attempt to explicitly resolve the spatial multi-phase structure of the ISM on small scales, but rather makes the assumption that crucial aspects of the global dynamical behaviour of the ISM can be characterised by an effective "sub-resolution" model that uses only spatially averaged properties to describe the medium. In essence, by adopting a *statistical* formulation, we seek to account for the impact of unresolved physics on scales that are resolved.

In our hybrid approach, each SPH fluid element represents a region in the ISM, whose properties are obtained from a suitable coarse-graining procedure. This is analogous to the N-body representation of collisionless fluids, but here the structure of the unresolved matter is more complex. In particular, we picture the medium as a fluid comprised of condensed clouds in pressure equilibrium with an ambient hot gas. The clouds supply the material available for star formation. For these hybrid-particles, the equations of hydrodynamics are only followed for the ambient gas. The cold clouds are subject to gravity, add inertia, and participate in mass and energy exchange processes with the ambient gas phase. These processes are computed on a particle by particle basis in terms of simple differential equations using a specific model for the physics of the ISM. Here, we attempt to incorporate some of the key aspects of the theoretical picture of the ISM outlined by McKee & Ostriker (1977).

In the following, ρ_h denotes the local density of the hot ambient gas, ρ_c is the density of cold clouds, $\rho_\star$ the density of stars, and $\rho = \rho_h + \rho_c$ is the total gas density. Individual molecular clouds and stars cannot be resolved, thus ρ_c and $\rho_\star$ represent averages over small regions of the ISM. We implicitly assume that such a coarse-graining procedure has been carried out, and we will formulate the interactions between the phases assuming that the regions used to define the averages are of constant volume. In our model, the average thermal energy per unit volume of the gas can then be written as $\epsilon = \rho_h u_h + \rho_c u_c$, where u_h and u_c are the energy per unit mass of the hot and cold components, respectively.

We model three basic processes that drive mass exchange between the phases. These are star formation, cloud evaporation due to supernovae, and cloud growth due to cooling. We discuss these processes in turn, focusing first on self-regulated, "quiescent" star formation. Later, we will extend the model to include additional processes leading to the development of galactic winds. For simplicity of presentation, we will omit adiabatic terms in the following definition of the model.

We assume that star formation converts cold clouds into stars on a characteristic timescale $t_\star$, and that a mass fraction β of these stars are short-lived and instantly die as supernovae. This can be described by:

$$\frac{\mathrm{d}\rho_\star}{\mathrm{d}t} = \frac{\rho_c}{t_\star} - \beta\frac{\rho_c}{t_\star} = (1 - \beta)\frac{\rho_c}{t_\star}. \tag{1}$$

In principal, there is a time delay between star formation events and associated supernovae equal to the approximate lifetime of massive stars ($\sim 3 \times 10^7$ years). However, for the quiescent mode of star formation, self-regulation is established so quickly that this time delay can be neglected.

Star formation therefore depletes the reservoir of cold clouds at the rate $\rho_c/t_\star$, and leads to an increase in the mass of the ambient phase as $\beta\rho_c/t_\star$, because we assume that ejecta from supernovae are returned as hot gas. The parameter β is the mass fraction of massive stars ($> 8M_\odot$)

formed for each initial population of stars and hence depends on the adopted stellar initial mass function (IMF). For a Salpeter IMF (1955) with slope -1.35 and upper and lower limits of $40\,\mathrm{M}_\odot$ and $0.1\,\mathrm{M}_\odot$, respectively, it has the value $\beta = 0.106$. We will typically adopt $\beta = 0.1$, and note that our results are not particularly sensitive to this choice.

In addition to returning gas (enriched with metals) to the ambient phase of the ISM, supernovae also release energy. The precise amount of this energy depends on the IMF. For the canonical value of 10^{51} ergs per supernova, we expect an average return of $\epsilon_{\mathrm{SN}} = 4 \times 10^{48}$ ergs $\mathrm{M}_\odot^{-1}$ for each solar mass in stars formed for the IMF adopted here. The heating rate due to supernovae is hence

$$\frac{\mathrm{d}}{\mathrm{d}t}(\rho_h u_h)\Big|_{\mathrm{SN}} = \epsilon_{\mathrm{SN}}\frac{\mathrm{d}\rho_\star}{\mathrm{d}t} = \beta u_{\mathrm{SN}}\frac{\rho_c}{t_\star}, \qquad (2)$$

where $u_{\mathrm{SN}} \equiv (1-\beta)\beta^{-1}\epsilon_{\mathrm{SN}}$ may be expressed in terms of an equivalent "supernova temperature" $T_{\mathrm{SN}} = 2\mu u_{\mathrm{SN}}/(3k) \simeq 10^8$ K.

In our formulation, we assume that the feedback energy from supernovae directly heats the ambient hot phase. In addition, we suppose that cold clouds are evaporated inside the hot bubbles of exploding supernovae, essentially by thermal conduction, thereby returning material from condensed clouds to the ambient gas. We take the total mass of clouds that are evaporated to be proportional to the mass in supernovae themselves, viz.

$$\frac{\mathrm{d}\rho_c}{\mathrm{d}t}\Big|_{\mathrm{EV}} = A\beta\frac{\rho_c}{t_\star}. \qquad (3)$$

The efficiency A of the evaporation process is expected to be a function of the local environment. For simplicity, we will only take the expected theoretical dependence on density, $A \propto \rho^{-4/5}$, into account (McKee & Ostriker, 1977). We will not try to estimate the evaporation efficiency from first principles, but rather treat its normalisation as a parameter. As we argue below, the range of permissible values for A is limited once we require a plausible temperature structure for the ISM.

Finally, we invoke a process by which cold clouds come into existence and grow. We assume that a thermal instability operates in the region of coexistence between the cold and hot phases, leading to mass exchange between ambient gas and cold clouds (Field, 1965; Field et al., 1969; Begelmann & McKee, 1990). In particular, we argue that radiative energy loss by the hot gas leads to a corresponding growth of the clouds, i.e. the energy radiated cools gas from the temperature of the hot phase to that of the cold phase and thus gives rise to a growth in the mass of cold clouds. This mass flux is thus:

$$\frac{\mathrm{d}\rho_c}{\mathrm{d}t}\Big|_{\mathrm{TI}} = -\frac{\mathrm{d}\rho_h}{\mathrm{d}t}\Big|_{\mathrm{TI}} = \frac{1}{u_h - u_c}\Lambda_{\mathrm{net}}(\rho_h, u_h). \qquad (4)$$

Note that we assume that the temperatures of and total volumes occupied by the hot and cold phases remain constant during cloud growth. We compute the cooling function Λ_{net} from the radiative processes appropriate for a primordial plasma of hydrogen and helium essentially as described by Katz et al. (1996). The abundances of the various ionisation states of H and He are computed explicitly, under the assumption of ionisation equilibrium in the presence of an external UV background field, which we here take to be a modified Haardt & Madau (1996) spectrum with reioni-

sation taking place at redshift $z \simeq 6$ (for details, see Davé et al., 1999).

The minimum temperature the gas can reach due to the radiative cooling processes we include is about 10^4 K, at which point the gas becomes neutral, and further cooling would require molecular cooling or that metals be present. In fact, real molecular clouds will form cores that are much colder than 10^4 K. However, in our present statistical formulation we neglect the internal structure of the clouds. Their exact thermal energy content will be unimportant in the current model as long as $u_h \gg u_c$, where we identify u_h with the hot intercloud medium resulting from supernova remnants at temperatures around $\sim 10^5 - 10^7$ K. We will typically assume a temperature of $T_c \simeq 1000$ K for the cold clouds, but note that the results do not depend on this choice for $T_c \ll 10^4$ K.

In the following, we will use a factor f to differentiate between situations where the thermal instability is assumed to be operating ($f = 0$), and regions where it is ineffective and ordinary cooling takes place ($f = 1$). In general, the gas can be expected to exhibit thermally unstable behaviour if the cooling rate is a declining function of temperature. For a primordial mixture of gas, this is the case roughly in the range $T \approx 10^5 - 10^6$ K, while for metal-enriched gas the minimum of the cooling curve shifts to higher temperatures, up to a few times 10^7 K. We thus require that the temperature of the ambient gas is above 10^5 K. For the onset of the thermal instability itself, we chose a simple density threshold criterion, i.e. $f = 0$ for $\rho > \rho_{\mathrm{th}}$, and $f = 1$ otherwise. This is motivated by the observed threshold behaviour of star formation (Kennicutt, 1989). Note that star formation will proceed only once clouds can form; i.e. when the gas density exceeds ρ_{th}.

Quantitatively, the rates at which the masses of the hot and cold phases evolve can be written as:

$$\frac{\mathrm{d}\rho_c}{\mathrm{d}t} = -\frac{\rho_c}{t_\star} - A\beta\frac{\rho_c}{t_\star} + \frac{1-f}{u_h - u_c}\Lambda_{\mathrm{net}}(\rho_h, u_h), \qquad (5)$$

$$\frac{\mathrm{d}\rho_h}{\mathrm{d}t} = \beta\frac{\rho_c}{t_\star} + A\beta\frac{\rho_c}{t_\star} - \frac{1-f}{u_h - u_c}\Lambda_{\mathrm{net}}(\rho_h, u_h). \qquad (6)$$

In both of these equations, the first term on the right hand side describes star formation and feedback, the second cloud evaporation, and the third the growth of clouds due to radiative cooling of the gas.

We now consider the energy budget of the gas, which we write as

$$\frac{\mathrm{d}}{\mathrm{d}t}(\rho_h u_h + \rho_c u_c) = -\Lambda_{\mathrm{net}}(\rho_h, u_h) + \beta\frac{\rho_c}{t_\star}u_{\mathrm{SN}} - (1-\beta)\frac{\rho_c}{t_\star}u_c, (7)$$

where Λ_{net} is the radiative cooling (or heating) function for the ambient hot medium. Only the ambient gas is assumed to be subject to radiative processes. The second term describes the non-gravitational energy injected by exploding supernovae. Finally, the third term describes the loss of energy in the gaseous phase due to material that is locked up in collisionless stars. The loss term arises because we assume that the material that is converted into stars is at the temperature of the cold clouds.

Within the framework of our model assumptions, we can split the energy equation into two separate relations for the thermal budget of the hot and cold components:

$$\frac{\mathrm{d}}{\mathrm{d}t}(\rho_c u_c) = -\frac{\rho_c}{t_\star}u_c - A\beta\frac{\rho_c}{t_\star}u_c + \frac{(1-f)u_c}{u_h - u_c}\Lambda_{\mathrm{net}}, \qquad (8)$$

$$\frac{\mathrm{d}}{\mathrm{d}t}(\rho_h u_h) = \beta\frac{\rho_c}{t_\star}(u_{\mathrm{SN}} + u_c) + A\beta\frac{\rho_c}{t_\star}u_c - \frac{u_h - fu_c}{u_h - u_c}\Lambda_{\mathrm{net}}. \; (9)$$

In these equations, the first term on the right hand side describes the effects of star formation and supernovae, the second accounts for cloud evaporation, and the third term the impact of thermal instability.

We assume that the cold clouds are at a fixed temperature, and so u_c will be treated as constant. Consequently, the above equations imply that the temperature of the hot phase will evolve according to

$$\rho_h\frac{\mathrm{d}u_h}{\mathrm{d}t} = \beta\frac{\rho_c}{t_\star}(u_{\mathrm{SN}} + u_c - u_h) - A\beta\frac{\rho_c}{t_\star}(u_h - u_c) - f\Lambda_{\mathrm{net}}. (10)$$

This is one of the basic equations that is integrated in the simulation code, augmented of course by terms coming from the external work done by pressure forces and viscous effects. In practice, we follow the evolution of the entropy of the hot phase in our code, rather than the thermal energy, for numerical reasons that are discussed by Springel & Hernquist (2002a).

An inspection of equation (10) reveals some interesting properties of our model. Suppose that the thermal instability is operating ($f = 0$), in which case the temperature of the hot phase changes only due to star formation and feedback. In fact, as long as star formation is active, the temperature will evolve towards

$$u_h = \frac{u_{\mathrm{SN}}}{A + 1} + u_c. \qquad (11)$$

Deviations from this temperature decay on a timescale

$$\tau_h = \frac{t_\star \rho_h}{\beta(A + 1)\rho_c}. \qquad (12)$$

Thus, provided star formation is sufficiently rapid compared to adiabatic heating or cooling due to gas motions, the temperature of the hot phase will be maintained at the value set by equation (11), which is *independent* of the star formation timescale $t_\star$. Since usually $A \gg 1$ and $u_{\mathrm{SN}}/A \gg u_c$ this temperature is in practice just given by $u_h \simeq u_{\mathrm{SN}}/A$. For a supernova temperature of 10^8 K and $A \sim 100$, the self-regulated temperature of the hot diffuse phase of the ISM will thus be maintained at $\sim 10^6$ K.

A further interesting consequence of our feedback model is that it leads to self-regulated star formation. Owing to evaporation, star formation reduces the density in cold clouds, lowering the star formation rate. On the other hand, a higher density of hot gas leads to an increase in the cooling rate, and hence to more rapid replenishing of clouds, increasing the star formation rate. In this manner, a self-regulated cycle of star formation is established where, in equilibrium, the growth of clouds is balanced by their evaporation due to supernova feedback.

This condition can be seen in more detail by considering equation (7). In the self-regulated regime, we expect the effective pressure of the medium

$$P_{\mathrm{eff}} = (\gamma - 1)(\rho_h u_h + \rho_c u_c) \qquad (13)$$

to be constant in time. This condition implies

$$\frac{\rho_c}{t_\star} = \frac{\Lambda_{\mathrm{net}}(\rho_h, u_h)}{\beta u_{\mathrm{SN}} - (1 - \beta)u_c}. \qquad (14)$$
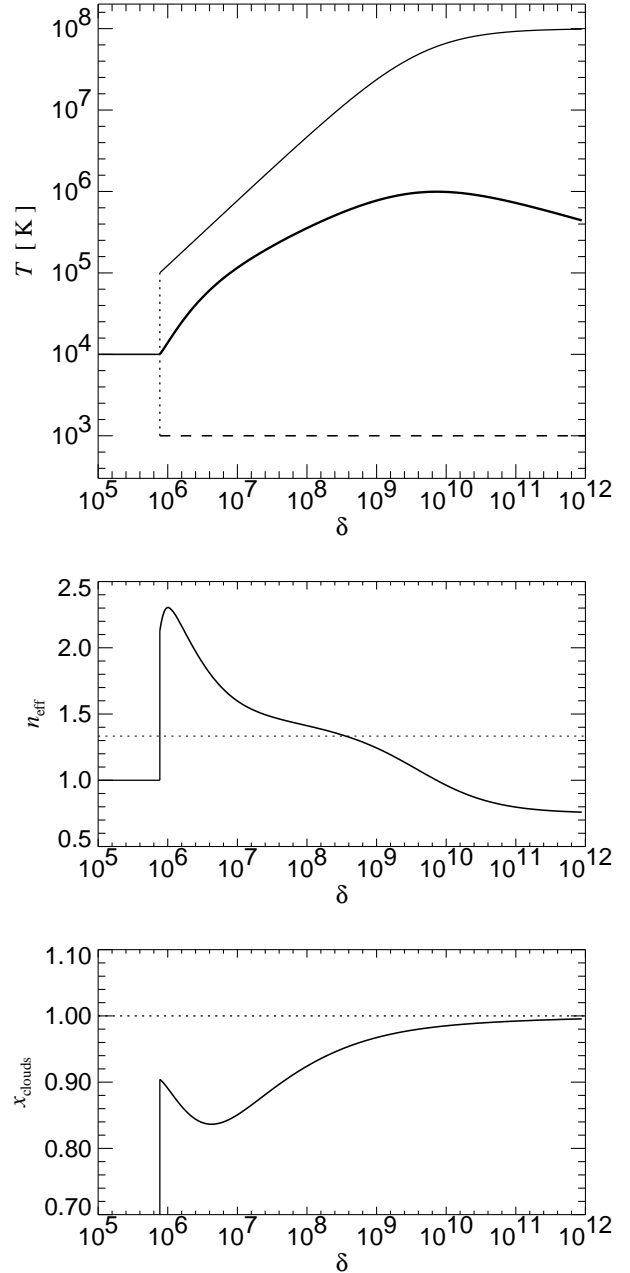

Figure 1. Top panel shows the temperature structure of the multi-phase medium as a function of baryonic overdensity (assuming $\Omega_b = 0.04$). Below a density of $\delta \simeq 8 \times 10^5$, star formation does not occur and the gas is treated as a single-phase fluid, with a temperature that is maintained close to 10^4 K by cooling and UV-heating. When star formation sets in, a hot ambient medium develops (thin solid line), and cold clouds are present at a fiducial temperature of 10^3 K (dashed). The mass-weighted effective temperature (thick solid line) is continuous at the onset of star formation, and can be interpreted in terms of an effective pressure P_{eff}. In the middle panel, we plot the local polytropic index $n_{\mathrm{eff}} = \mathrm{d}\log P_{\mathrm{eff}}/\mathrm{d}\log\rho$ of the resulting effective equation of state. The bottom panel shows the mass fraction in cold clouds as a function of overdensity.

Using $\Lambda_{\rm net}(\rho_h, u_h) = [\rho_h/\rho]^2 \Lambda_{\rm net}(\rho, u_h)$, we thus obtain an expression for the expected ratio of masses in the cold and hot phases, viz.

$$\frac{\rho_c}{\rho_h} = \frac{\rho_h}{\rho}\, y, \qquad (15)$$

where we have defined

$$y \equiv \frac{t_\star \Lambda_{\rm net}(\rho, u_h)}{\rho\, [\beta u_{\rm SN} - (1-\beta)u_c]}. \qquad (16)$$

Note that y is a function only of ρ in the self-regulated regime, provided that $t_\star$ and A depend only on density. We can then express the mass fraction

$$x \equiv \frac{\rho_c}{\rho} \qquad (17)$$

of cold clouds as

$$x = 1 + \frac{1}{2y} - \sqrt{\frac{1}{y} + \frac{1}{4y^2}}\,. \qquad (18)$$

The effective pressure of the gas will then take on the value

$$P_{\rm eff} = (\gamma - 1)\rho\,[(1-x)u_h + x u_c]\,, \qquad (19)$$

where the term in square brackets is the effective mass-weighted "temperature" $u_{\rm eff}$ of the medium.

In Figure 1, we show the density dependence of this effective temperature, and of the temperatures of the hot and cold components in our multi-phase model of the ISM. Also shown is the mass fraction of gas in cold clouds, and the local logarithmic slope $n_{\rm eff}$ of the effective equation of state $P_{\rm eff}(\rho)$ of the star-forming medium. It is clear that the functional dependence of $P_{\rm eff}$ on density is particularly important for the dynamical stability of star-forming regions. For $n_{\rm eff} > 4/3$, the effective pressure can provide enough vertical thickening to stabilise gaseous disks against rapid break-up into clumps due to dynamical instabilities.

3   SELECTING PARAMETERS

Following McKee & Ostriker (1977), we express the density dependence of the supernova evaporation parameter A as

$$A(\rho) = A_0 \left(\frac{\rho}{\rho_{\rm th}}\right)^{-4/5}, \qquad (20)$$

where $\rho_{\rm th}$ and A_0 are parameters of our model. To specify the star formation timescale, $t_\star$, we make the common assumption that this quantity is proportional to the local dynamical time of the gas. This plausible choice results in a Schmidt-type law for the dependence of the star formation rate on density, as observed. We thus set

$$t_\star(\rho) = t_0^\star \left(\frac{\rho}{\rho_{\rm th}}\right)^{-1/2}, \qquad (21)$$

where $t_0^\star$ is an additional parameter of the model.

Before we study the properties of our model in detail, we discuss how its free parameters can be constrained. To this point, we have introduced two parameters that depend on the IMF, β and $u_{\rm SN}$, and three parameters that determine the regulation of the multi-phase medium due to star formation; these are $\rho_{\rm th}$, A_0, and $t_0^\star$.

For the purposes of this work, we neglect uncertainties in the IMF and treat β and $u_{\rm SN}$ as known constants. However, the other three parameters are crucially important to the behaviour of the model. We proceed by first requiring that at the onset of thermal instability, the equilibrium temperature of the hot medium is such that the thermal instability in fact becomes operative. This means that the cooling function should start to fall at this temperature, which happens at $\simeq 10^5\,$K. We thus require that

$$T_{\rm SN}/A_0 = 10^5\ {\rm K}, \qquad (22)$$

which fixes A_0 to a value of $A_0 \simeq 1000$.

Next, we argue that the effective pressure of the gas should be a continuous function of density at the onset of the regime of self-regulated star formation. The gas just below the threshold will have cooled down to $10^4\,$K, where it becomes neutral. Further cooling could happen only due to less efficient molecular cooling processes that we ignore. (For now, we also neglect cooling due to metals, which could however become significant once the gas becomes chemically enriched from star formation.) Hence we impose the condition $u_{\rm eff}(\rho_{\rm th}) = u_4$, where u_4 is the specific energy corresponding to a temperature of $10^4\,$K. Based on the equations for the self-regulated regime, we thus have

$$\rho_{\rm th} = \frac{x_{\rm th}}{(1-x_{\rm th})^2}\, \frac{\beta u_{\rm SN} - (1-\beta)u_c}{t_\star^0 \Lambda(u_{\rm SN}/A_0)}, \qquad (23)$$

which sets the density threshold $\rho_{\rm th}$ for a given a value of $t_0^\star$. Here, $x_{\rm th} = 1 + (A_0+1)(u_c - u_4)/u_{\rm SN} \simeq 1 - A_0 u_4/u_{\rm SN}$ is the mass fraction in clouds at the threshold, and Λ is defined by $\Lambda(\rho, u) = \Lambda_{\rm net}(\rho, u)/\rho^2$, such that Λ looses its dependence on density for temperatures high compared to $10^4\,$K.

We have thus reduced the description of our model to one free parameter, the star formation timescale $t_0^\star$. It is clear that this parameter sets the overall gas consumption timescale, which is, in principle, well-constrained by observations of the efficiency of star formation.

Observationally, there appears to be a tight correlation between disk-averaged measurements of the star formation rate per unit area and the gas surface density, a "global Schmidt-law", given by Kennicutt (1998) as

$$\Sigma_{\rm SFR} = (2.5 \pm 0.7) \times 10^{-4} \left(\frac{\Sigma_{\rm gas}}{{\rm M}_\odot {\rm pc}^{-2}}\right)^{1.4 \pm 0.15} \frac{{\rm M}_\odot}{{\rm yr\,kpc}^2}. (24)$$

This correlation is valid from typical disk-averaged gas densities of $10\,{\rm M}_\odot {\rm pc}^{-2}$ in normal spirals to gas densities as high as $10^5\,{\rm M}_\odot {\rm pc}^{-2}$ in the central regions of starbursting galaxies. Roughly the same law also appears to hold locally for azimuthally averaged gas densities and star formation rates, although perhaps with a slightly smaller amplitude than the one given by equation (24). In addition, there is a clear threshold behaviour for star formation, with $\Sigma_{\rm SFR}$ very rapidly falling at densities below $\sim 10\,{\rm M}_\odot {\rm pc}^{-2}$ (Kennicutt, 1989, 1998; Martin & Kennicutt, 2001). It has been suggested that the threshold might be related to the onset of gravitational instabilities in the disk, but presently the evidence for this argument remains inconclusive.

By modelling individual galaxies, we will directly try to fit the Schmidt-law of equation (24), using however a slope of 1.5, which prompts us to lower the normalising coefficient in front by a factor of 2. This correction results when changing the best-fit slope to 1.5 and simultaneously requiring
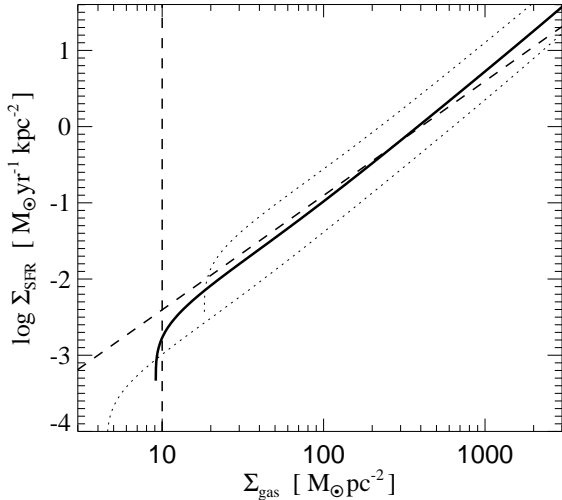
Figure 2. Star formation rate per unit area versus gas surface density in a star-forming disk of gas. The dashed inclined line shows the Kennicutt law of equation (25), with the vertical line drawn to indicate the observational cut-off in the star formation rate. The solid and dotted lines have been computed numerically by solving the equations of hydrodynamic equilibrium together with our multi-phase model for self-gravitating sheets of gas. The solid line shows the result for $t_0^\star = 2.1\,\mathrm{Gyr}$, the lower dotted line is obtained for $t_0^\star = 8.4,\mathrm{Gyr}$, and the upper dotted line for $t_0^\star = 0.53\,\mathrm{Gyr}$.

Figure 3. Star formation rate per unit area versus gas surface density in a self-consistent simulation of a disk galaxy which quiescently forms stars. The symbols show azimuthally averaged measurements obtained for our fiducial choice of $t_0^\star = 2.1\,\mathrm{Gyr}$. The dashed inclined line gives the Kennicutt law of equation (25), and the vertical line marks the observed cut-off of star formation.

the star formation rate to remain unchanged at the intermediate density value of $10^3\,\mathrm{M_\odot pc^{-2}}$. The resulting local Schmidt-law then provides a good fit to the azimuthal data of 21 spirals presented in Fig. 3 of Kennicutt (1998). The observational constraint we thus try to match can also be expressed as a gas consumption timescale, taking the form

$$t_{\mathrm{SFR}} = \frac{\Sigma_{\mathrm{gas}}}{\Sigma_{\mathrm{SFR}}} = 3.2\,\mathrm{Gyr} \left(\frac{\Sigma_{\mathrm{gas}}}{10\,\mathrm{M_\odot\,pc^{-2}}} \right)^{-0.5}. \qquad (25)$$

At the threshold for the onset of star formation, this thus indicates a timescale of about 3.2 Gyr, becoming shorter towards higher densities. This compares well with the cited median gas consumption timescales of 2.1 Gyr (Kennicutt, 1998) and 2.4 Gyr (Rownd & Young, 1999).

In Figure 2, we show the relation between star formation density and gas surface density predicted by our multi-phase model for various choices of $t_0^\star$. The curves have been computed by solving the equations of hydrostatic equilibrium for self-gravitating layers of gas with varying surface density. Clearly, the amplitude of the star formation rate is very sensitive to the value of $t_0^\star$, with $t_0^\star = 2.1\,\mathrm{Gyr}$ providing a good fit to the Kennicutt law.

Once the amplitude of star formation has been matched by adjusting $t_0^\star$, the slope and the cut-off obtained can be used as additional checks on the applicability of our model. The slope is matched quite well, even though this is not entirely trivial because it requires that the vertical structure that develops under the action of P_{eff} for the self-gravitating, star-forming sheet of gas leads to star formation rates per unit area which are compatible with the observed slope of the Schmidt-law. Interestingly, the cut-off induced by the
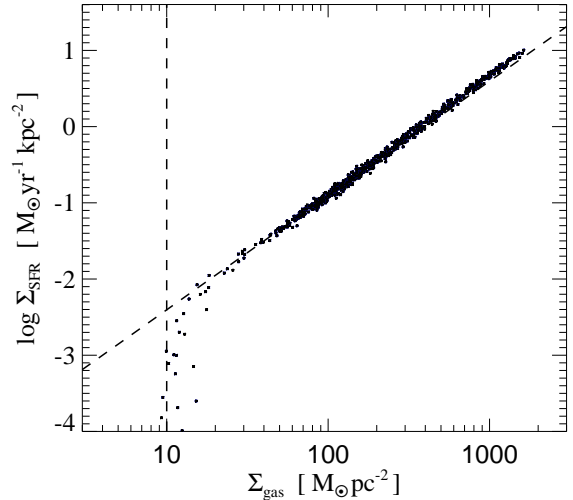
best-fit value of $t_0^\star$ also lies approximately in the right location. It is presently unclear whether this has any profound significance, or whether it is just a fortunate coincidence in the present simple model. Recall that the cut-off in the model is induced by an imposed physical density threshold ρ_{th} for the onset of cloud formation, and that this density is tied to the value for the star formation timescale.

Finally, we examine how well full three-dimensional simulations of spiral galaxies obey the Kennicutt law that we used to set the star formation timescale. In Figure 3, we show azimuthally averaged measurements obtained for our fiducial choice of $t_0^\star = 2.1\,\mathrm{Gyr}$ in a compound galaxy consisting of a dark halo, and a star-forming gaseous disk. There is good agreement with the corresponding analytic curve in Fig. 2, validating the numerical implementation of the multi-phase model in our simulation code.

4   WINDS AND STARBURSTS

4.1   Winds

As summarised above, our multi-phase model leads to the establishment of a physically motivated and numerically well controlled regulation cycle for star formation in gas that has cooled and collapsed to high baryonic overdensities. Gas contained in dark matter haloes can thus cool and settle into rotationally supported disks where the baryons are gradually converted into stars, at a rate consistent with observations of local disk galaxies. In this model, the thickness and the star formation rates of gaseous disks are regulated by supernova feedback, which essentially provides finite pressure support to the star forming ISM, thereby preventing it from collapsing gravitationally to exceedingly high densities, and

also allowing gaseous disks to form that are reasonably stable against axisymmetric perturbations.

However, it is clear that the model we have outlined so far will not be able to account for the rich phenomenology associated with starbursts and galactic outflows, which are observed at both low (e.g. Heckman et al., 1995; Bland-Hawthorn, 1995; Lehnert & Heckman, 1996; Dahlem et al., 1997; Heckman et al., 2000) and high redshifts (e.g. Frye et al., 2002; Pettini et al., 2000, 2001). This is because our multi-phase model by itself offers no obvious route for baryons to climb out of galactic potential wells *after* having collapsed into them due to cooling. Note that for the hybrid model of quiescent star formation we explicitly assume that the cold clouds and the hot surrounding medium remain tightly coupled at all times. The high entropy gas of supernova remnants is thus trapped in potential wells by being tied into a rapid cycle of cloud formation and evaporation. In principal, tidal stripping of enriched gas in galaxy interactions (Gnedin & Ostriker, 1997) could lead to a transport of enriched gas back into the low-density IGM. However, high-resolution simulations of galaxy collisions (Barnes, 1988; Barnes & Hernquist, 1992; Hernquist, 1992, 1993) have shown that such dynamical removal of gas from the inner regions of galaxies appears to be rather inefficient, especially for the deep potential wells expected for haloes in CDM universes (Springel & White, 1999).

On the other hand, it is becoming increasingly clear that galactic winds and outflows may play a crucial role not only in chemically enriching and possibly heating the IGM (Nath & Trentham, 1997; Madau et al., 2001; Aguirre et al., 2001a,b,c), in polluting the IGM with dust (Aguirre, 1999a,b), and in enriching the intracluster and intragroup medium, but may also be an important mechanism in regulating star formation on galactic scales (Scannapieco et al., 2000; Scannapieco & Broadhurst, 2001a,b). Since winds can reheat and transport collapsed material from the center of a galaxy back to its extended dark matter halo and even beyond, they can help to reduce the overall cosmic star formation rate to a level consistent with observational constraints. Because radiative cooling is very efficient at high redshifts and in small haloes (White & Rees, 1978; White & Frenk, 1991), numerical simulations of galaxy formation typically either overproduce stars compared with the luminosity density of the universe, or harbour too much cold gas in galaxies. The self-regulated model we present above will also suffer from this problem, because it does not drastically alter the total amount of gas that cools. It is plausible, however, that galactic winds may solve this "overcooling" problem, provided that they can expel sufficient quantities of gas from the centres of low-mass galaxies. Removal of such low-angular momentum material may also help to resolve the problem of disk sizes being too small in CDM theories (Navarro & White, 1994b; Navarro & Steinmetz, 2000; Binney et al., 2001). Note that semi-analytic models of galaxy formation must also invoke feedback processes that reheat cold gas and return to the extended galactic halo or eject it altogether.

We are thus motivated to extend our feedback model to account for galactic winds driven by star formation. Winds have been investigated in a number of theoretical studies (Mac Low & Ferrara, 1999; Aguirre et al., 2001a,b,c; Efstathiou, 2000; Madau et al., 2001; Scannapieco et al.,

2001, among others), but the mechanism by which galactic outflows originate is not yet well understood. In the star-forming multi-phase medium, it is plausible that not all of the hot gas in supernova remnants will remain confined to the disk by being quickly used up to evaporate cold clouds. Instead, supernova bubbles close to the surface of a star-forming region may break out of a disk and vent their hot gas into galactic haloes. As a result, a galactic-scale wind associated with star formation may develop. Note that this process does not necessarily require a prominent starburst, but could be a common phenomenon even with quiescent star formation (Efstathiou, 2000). In the latter case, winds may often not be strong enough to escape from all but the smallest galaxies, but they can nevertheless represent a crucial process for transporting metals and energy released by supernovae into the extended galactic halo.

Unfortunately, our understanding of the small-scale hydrodynamics that is actually responsible for driving winds is crude, although high-resolution simulations of starbursts (Mac Low & Ferrara, 1999) provide some clues about the physics. Here, we will not attempt to formulate a detailed theory for the production of winds, but will rather use a phenomenological approach that can easily be combined with our model for star formation and feedback. To this end, we will parameterise the winds in analogy to Aguirre et al. (2001b), who studied wind propagation and metal enrichment of the IGM using detailed analytic models applied to a sequence of simulation time slices. Their phenomenological model of winds was constructed to be physically and energetically plausible, to be simple, and to be constrained by observational data to the extent possible, an approach we will also follow.

We start by assuming that the disk mass-loss rate that goes into a wind, $\dot{M}_{\rm w}$, is proportional to the star formation rate itself, viz.

$$\dot{M}_{\rm w} = \eta \dot{M}_{\star} \,, \tag{26}$$

where η is a coefficient of order unity. In fact, Martin (1999) presents observational evidence that the disk mass-loss rates of local galaxies are of order the star formation rates themselves, with $\dot{M}_{\rm w}/\dot{M}_{\star} \sim 1-5$, and without evidence for any dependence on galactic rotation speed. Note that $\dot{M}_{\rm w}$ just describes the rate at which gas is lost from a disk and fed into a wind. Whether or not this material will be able to escape from the halo will then depend on a number of factors: the velocity to which the gas is accelerated, the amount of intervening and entrained gas, and the depth of the potential well of the halo. If the wind is slow and the halo is of sufficient mass, the gas ejected from the disk will remain bound to the halo, and may later fall back to the star-forming region, giving rise to a galactic "fountain." On the other hand, even a slow wind may escape dwarf galaxies and, at sufficiently high redshift, can potentially pollute a large volume without overly perturbing the thermal structure of the low-density IGM. Note that for values of η above unity, a wind is expected to greatly suppress star formation in galaxies that are of low enough mass to allow the wind to escape. We will adopt $\eta = 2$ in our fiducial wind model, consistent with the observations of Martin (1999).

We further assume that the wind carries a fixed fraction χ of the supernova energy. Equating the kinetic energy in the wind with the energy input by supernovae,

$$\frac{1}{2}\dot{M}_{\mathrm{w}}v_{\mathrm{w}}^2 = \chi\epsilon_{\mathrm{SN}}\dot{M}_\star, \tag{27}$$

we obtain the wind's velocity when it leaves the disk as

$$v_{\mathrm{w}} = \sqrt{\frac{2\beta\chi u_{\mathrm{SN}}}{\eta(1-\beta)}}. \tag{28}$$

We will treat χ as a further parameter of the wind model. While it cannot be larger than 1 in the present formalism, it is nevertheless to be expected that the wind energy constitutes a sizable fraction of the overall supernova energy input. We will assume $\chi = 0.25$ in most of the test simulations discussed in this paper. Note that it should in principle be possible to use observations of the cosmic star formation history or the metal enrichment of the IGM to constrain this parameter. We do not explicitly model a distribution of wind velocities in this study. Of course, some variation of the local wind speed will be automatically produced by the dynamics of local gas interactions.

4.2 Starbursts

We have shown that our hybrid model leads to an efficient self-regulation of star formation, which can be understood in terms of an effective equation of state. In general, the model is thus best viewed as describing quiescent star formation, where the star formation rate will in general only gradually accelerate when the gas density is increased, in accordance with the empirical Schmidt law. The winds we have introduced as an extension of this model will not change this picture. We specifically postulate that a wind leaves a star-forming region without significantly perturbing it dynamically, and our numerical implementation of wind formation is designed to ensure this behaviour. Winds thus merely reduce the amount of gas available for star formation. Depending on the depth of the potential well, the gas may or may not come back to the galactic disk at a later time and become available for star formation again.

It is interesting to note, however, that we expect the quiescent mode of star formation to eventually become "explosive" (i.e. very rapid) for sufficiently high gas densities. Physically, it is plausible that self-regulation should break down at high densities. In the self-regulated regime, cold clouds are constantly being formed and evaporated. If clouds are not replenished by cooling, they will be consumed on a timescale $t_c = t_\star/(\beta A) = (\rho/\rho_{\mathrm{th}})^{3/10}t_0^\star/(\beta A_0)$. This timescale t_c describes the rate at which clouds are reprocessed. At the onset of star formation, it is about a factor 100 shorter than the star formation timescale itself, on the order of a few times 10^7 years. However, at higher densities, clouds are reprocessed more slowly, and eventually t_c will become larger than the maximum lifetime of individual clouds, which is estimated to be as high as 10^8 yr for giant molecular clouds. At this point, it will become difficult to maintain tight self-regulation because the clouds will not survive long enough to await evaporation. Instead they may all collapse and form stars on the timescale of their lifetime, i.e. the timescale of star formation will suddenly become shorter in this regime and deviate from the scaling we have assumed so far.

Since it is unclear how this transition to accelerated star formation proceeds in detail, we refrain from modelling it explicitly in this study. However, we remark that already

the effective pressure model discussed so far shows a possibility for run-away star formation, for purely dynamical reasons. Recall that the ISM is stabilised against gravitational collapse by the effective pressure provided in the multi-phase model. For sufficiently high densities, the corresponding equation of state eventually becomes soft. More specifically, there is a certain overdensity, where the local polytropic index falls below a slope of 4/3. It is well known that barotropic gas spheres with an index below this value are unstable. We thus expect that once we assemble a sufficiently large amount of cold gas, the effective pressure will be insufficient to stabilise the cloud against further gravitational collapse to much higher densities, leading to a run-away conversion of the gas into stars.

5 NUMERICAL IMPLEMENTATION

The hybrid multi-phase model outlined in Section 2 can be represented numerically in a number of different ways. Yepes et al. (1997) used an Eulerian hydro code, where the properties of the flow are discretised on a mesh. The mesh size provides a natural scale for the coarse-graining procedure inherent in our model. One may also discretise the *mass*, as is done in the Lagrangian SPH technique. Hultman & Pharasyn (1999) presented a first implementation of the approach of Yepes et al. (1997) using SPH.

We also employ SPH to implement our model, in the form of a modified and extended version of the parallel TreeSPH code GADGET (Springel et al., 2001b). Throughout, we will use the novel formulation of SPH that was recently derived by Springel & Hernquist (2002a), which manifestly conserves energy and entropy when appropriate, and greatly reduces numerical inaccuracies that otherwise can arise in poorly resolved cooling flows.

On a technical level, we have actually implemented two different methods for representing our star formation model in the code. In an "explicit" treatment, which we will describe first, each SPH particle can have three different mass components, describing "ordinary" ambient gas, cold clouds, and collisionless stars. The various processes of cloud formation, cloud evaporation and star formation are then explicitly followed in terms of mass exchange between these components of the hybrid particles.

However, because the self-regulation timescale is typically short compared to the dynamical and star formation timescales, the mass fraction contained in cold clouds at a given density can be obtained with good accuracy by just assuming the equilibrium value expected for self-regulation, where the latter can be worked out analytically. We can thus replace the explicit treatment with a simplified method based on these equilibrium values. Star particles can then be formed stochastically from the reservoir of clouds, thereby avoiding an artificial coupling of gas and collisionless stellar material. This idea forms the basis of our second method for implementing the multi-phase model, to be described after the explicit treatment.

5.1 Explicit implementation of the multi-phase model

In our explicit variant for implementing the multi-phase model, we describe each SPH hybrid-particle by a total mass m, a mass $m_\star$ in stars, a mass m_c in cold clouds, and an internal energy u_h in the ambient gas. The mass in the "ordinary" gas phase is therefore given by $m_h = m - m_\star - m_c$. Note that we here build up stellar mass gradually in each star-forming particle, unlike in the effective treatment discussed in the next section, which avoids the implied temporary coupling of gas and collisionless stellar material. Also note that most SPH particles in a cosmological simulation will never reach the high densities required for star formation, and will therefore have $m = m_h$, with u_h describing their normal thermal reservoir.

We compute the hydrodynamical forces in the usual manner, but take the pressure to be

$$P = (\gamma - 1)\rho(m_h u_u + m_c u_c)/(m_h + m_c), \tag{29}$$

and compute kernel-estimated densities with the gas mass $m - m_\star$ of each particle only. The stellar masses $m_\star$ add inertia to the particles and contribute to the source function of the gravitational field. Star formation is then treated in the code on a particle by particle basis in the following manner:

(i) For each timestep Δt, we first work out the mass of clouds that turns into stars and produces supernovae:

$$\Delta m_{\rm sf} = m_c \frac{\Delta t}{t_\star}. \tag{30}$$

(ii) If the thermal instability is active ($f = 0$), we then compute the new mass in the hot phase. To this end, we consider the Lagrangian analogue of equation (6):

$$\Delta m_h = \beta(A+1)\Delta m_{\rm sf} - \frac{\Lambda_{\rm net}}{u_h - u_c}\frac{m_h}{\rho_h}\Delta t, \tag{31}$$

and we solve this equation implicitly for the new mass m_h' in the following way:

$$m_h' = m_h + \beta(A+1)\Delta m_{\rm sf} - \frac{\Lambda_{\rm net}(\rho_h m_h'/m_h, u_h)}{u_h - u_c}\frac{m_h}{\rho_h}\Delta t \tag{32}$$

This guarantees stability even when m_h changes rapidly. In order to improve the robustness of the integration, we however do not allow m_h' to fall below half the value of m_h in a single step. If the thermal instability is not active, we simply have $m_h' = m_h + \beta(A+1)\Delta m_{\rm sf}$.

(iii) Once m_h' is determined, we can compute the mass that is actually transferred from the hot to the cold phase due to the thermal instability alone:

$$\Delta m_{\rm TI} = m_h + \beta(A+1)\Delta m_{\rm sf} - m_h'. \tag{33}$$

Note that $\Delta m_{\rm TI} = 0$ if the thermal instability is not operating. The mass evaporated by supernovae is

$$\Delta m_{\rm evap} = \beta A \Delta m_{\rm sf}. \tag{34}$$

(iv) The new masses of cold and hot phase can now be obtained as:

$$m_c' = m_c - \Delta m_{\rm sf} + \Delta m_{\rm TI} - \Delta m_{\rm evap} \tag{35}$$

$$m_h' = m_h + \beta\Delta m_{\rm sf} - \Delta m_{\rm TI} + \Delta m_{\rm evap} \tag{36}$$

And the new stellar mass is:

$$m_\star' = m_\star + (1 - \beta)\Delta m_{\rm sf} \tag{37}$$

Note that the total mass is conserved, $m_h' + m_c' + m_\star' = m_h + m_c + m_\star$, by construction.

(v) If the thermal instability is operating, the rate of change of internal energy of the ambient medium is given by the normal adiabatic term plus the contribution

$$\frac{{\rm d}u_h}{{\rm d}t} = \frac{\beta\Delta m_{\rm sf}[u_{\rm SN} + (A+1)(u_c - u_h)]}{m_h\Delta t} \tag{38}$$

from star formation and feedback. Otherwise, if ordinary cooling is active, the rate of change of internal energy additionally gets a contribution from the normal cooling function, with the latter being solved implicitly for the new temperature at the end of the timestep (Springel et al., 2001b).

Note that the coupling of the three phases can cause difficulties in certain situations. For example, if a hybrid particle is dynamically stripped from a star forming region and moves to an environment of lower density, the particle will at first have most of its gas mass still bound in cold clouds. These clouds will quickly be evaporated by residual star formation of the particle, provided its density has not fallen so rapidly that the star formation timescale has become very long. If this should happen, cloud material may escape to very low density, and survive there for a long time. In order to prevent this, we assume that all clouds are evaporated instantly if the density of a particle falls below $\rho_{\rm th}$, with the required energy extracted from the reservoir u_h. Star formation will thus be strictly confined to the regions $\rho > \rho_{\rm th}$, and all gas of lower density is just "ordinary" gas.

Somewhat more problematic is the tight coupling of the stellar material that has formed to the mass that still resides in gas. This is in principle unphysical, even though it may be a reasonable approximation in many cases, because the stars and the star-forming medium tend to move together, except in highly dynamic situations, as, for example, in major mergers. Nevertheless, it is clear that the explicit treatment described above requires a mechanism that eventually decouples the formed stellar material from the gas, otherwise one could obtain at late times large numbers of "gas" particles whose masses are dominated by their stellar components. In order to achieve such a decoupling, we turn a hybrid particle whose stellar mass has grown above its gas mass, i.e. for $m_\star \geq 0.5m$, into a star particle of mass $m_\star$. The rest of the mass, consisting of clouds and ambient gas, is distributed kernel-weighted among the SPH neighbours of the particle that is being converted. We distribute clouds and ambient mass separately, as well as the thermal energy in the ambient medium.

This mechanism maintains a roughly constant mass resolution, and it keeps the total particle number exactly constant. However, it is clear that subtle dynamical effects due to the temporary coupling of gaseous and stellar material may remain. This is one of the reasons why we prefer a simplified, "effective" implementation of the multi-phase model which we describe next.

5.2 Simplified treatment assuming self-regulation

According to equation (10), the ambient hot medium evolves towards an equilibrium temperature on a timescale given by equation (12), provided that the density is sufficiently

high for star formation to occur. This time is short compared to the star formation timescale; i.e. conditions for self-regulation are achieved quickly. In order to simplify the computation of the gasdynamics, it should, therefore, be a good approximation to assume that the conditions of self-regulated star formation always hold. In this case, the temperature of the ambient hot medium is simply given by equation (11), and the mass fraction in clouds follows from equations (16) and (18). This then also determines the star formation rate and the effective pressure (19) of each particle. In this way, we avoid treating the mass exchange processes explicitly, simplifying the code, making it faster, and reducing its storage requirements.

Additional advantages follow if the build-up of the stellar component is not described "smoothly" as in the explicit approach, but instead probabilistically with expectation value consistent with the star formation rate. The star formation rate of an SPH particle of current mass m is given by $\dot{M}_\star = (1 - \beta)\, x\, m/t_\star$. Given a timestep Δt, we spawn a new star particle of mass $m_\star = m_0/N_g$ once a random number drawn uniformly from the interval $[0, 1]$ falls below

$$p_\star = \frac{m}{m_\star} \left\{ 1 - \exp\left[-\frac{(1 - \beta)\, x \Delta t}{t_\star} \right] \right\}. \tag{39}$$

The initial phase-space variables of the new particle are copied from the gas particle, which in turn is reduced in mass by $m_\star$. Here, m_0 is the initial gas mass of each SPH particle, and N_g is an integer which gives the number of "generations" of stars each gas particle may form. If a gas particle has already spawned $N_g - 1$ stars, it will simply be turned into a star particle should it become the site of another star formation event.

Note that all the star particles will have identical masses in this approach. For choices of N_g in the range between 1 and about 4, one achieves good mass resolution for the stellar component, while simultaneously maintaining a reasonably constant mass resolution in the gaseous phase. For $N_g > 1$ the total number of particles increases due to star formation, but there is a firm upper bound to this number, and if only a small fraction of the baryons are turned into stars, as in cosmological simulations, the relative increase is moderate.

More important, there is no artificial dynamical coupling between the gas particles and the stars in this approach, because all the stellar mass is contained in independent star particles at all times, unlike in the explicit treatment, where each component is tied to hybrid gas-star particles. Another advantage is that the distribution of formation times of the star particles directly reflects the underlying star formation history, without any bias, thereby simplifying the analysis and interpretation of simulation outputs. The equal masses of star particles also keep possible mass segregation effects due to collisional relaxation to a minimum, and in the limit of very large N_g one naturally approaches the limit of continuous star formation.

$\Delta M_\star$ locked up in long-lived stars, the mass in metals returned is $\Delta M_{\text{met}} = p \Delta M_\star$, where p is the *yield*. Provided that these metals are well mixed with the local gas of mass M_g, and provided no gas enters or leaves the system (i.e. a closed-box) the metallicity $Z \equiv M_{\text{met}}/M_g$ will increase by $\Delta Z = p \Delta M_\star / M_g$ due to the formation of the stars. This already takes into account that some of the metals in the gas are also lost to the forming stars.

Here, we assume that each gas element locally behaves as a closed box, with metals being instantaneously mixed between clouds and ambient gas. The metallicity of a patch of the ISM will therefore increase during one timestep by

$$\Delta Z = (1 - \beta)\, p\, x\, \frac{\Delta t}{t_\star}, \tag{40}$$

where x is the local fraction of gas contained in cold clouds. For gas below the threshold density for star formation, we have $x = 0$ and the metallicity remains constant.

It is straightforward to follow the growth of the metallicity of each gas particle using equation (40), both for the explicit treatment of the multi-phase structure as described in section 5.1, or for the simplified "effective" method described in section 5.2. However, depending on the approach used, it is more problematic to define the metallicity of the star particles. In the explicit treatment, the stellar component is built up gradually, with stars being formed from gas of varying metallicity. The independent star particles that are eventually produced will then have a mass-weighted average of the metallicities of the gas elements from which they were formed. This complicates the interpretation of the metallicity distribution of these star particles, because it will not directly reflect the metallicity distribution obtained if star formation were instead always to immediately generate independent star particles.

In the probabilistic method of generating star particles, this problem does not arise. The metallicity of a newly spawned star particle is just given by the current metallicity of the star-forming gas particle. In this method, the expectation value of the total mass in metals found in gas and stars at any given time will be equal to the yield times the total mass in stars. Note that the effective model also avoids any metal diffusion, which can occur at a small level in the explicit treatment where remaining gas and metals are distributed among neighbouring particles once a gas particle is dissolved, with its hybrid stellar component being turned into a collisionless particle.

Although there is no efficient mechanism for metal diffusion in our model, metals can of course be transported along with the gas flow. In particular, winds may deposit metals far from where they were produced, leading, for example, to enrichment of the haloes of galaxies, or of the IGM. However, currently we do not yet include metal-line cooling in our code, hence the metallicity acts fundamentally only as a tracer variable without having any dynamical consequences. In future work, we plan to investigate effects that arise when this part of the model is refined.

5.3 Metal enrichment

Stellar winds and supernova explosions of massive stars enrich surrounding gas with metals (i.e. all elements heavier than helium). We assume that for each mass element

5.4 Wind formation

As discussed in Section 4, we assume that star formation can be accompanied by mass-loss from star-forming regions, giving rise to winds. There is strong observational evidence that

such winds exist, but the detailed physics underlying this phenomenon is unclear. But, even if there were a firm theoretical basis for understanding these winds, we currently lack the spatial resolution in our simulations to directly model the relevant physical processes. We are thus led to adopt a phenomenological treatment of how such winds are generated. At a technical level, we proceed in a similar way to the probabilistic method for spawning star particles.

During a timestep Δt, a gas particle is added to the wind if a uniformly distributed random number out of the interval $[0, 1]$ falls below

$$p_w = 1 - \exp\left[-\frac{\eta(1 - \beta)\, x \Delta t}{t_\star}\right]. \tag{41}$$

If this is the case, we modify the particle's velocity $\boldsymbol{v}$ according to

$$\boldsymbol{v}' = \boldsymbol{v} + v_w\, \boldsymbol{n}, \tag{42}$$

where v_w is the wind velocity given by equation (28). For the unit vector $\boldsymbol{n}$, we either select a random direction on the unit sphere (isotropic wind), or we choose a random orientation along the direction $\boldsymbol{v} \times \nabla\phi$, where ϕ is the gravitational potential ("axial" wind). If the latter scheme is chosen, the wind particles are preferentially ejected along the rotation axis of a spinning object. This mimics the expected preference of wind ejection to occur in a direction orthogonal to rotationally flattened, disk-like galaxies. However, even for an isotropic wind the presence of a dense disk will lead to a bipolar wind pattern, simply because the wind can propagate much more easily in the direction orthogonal to the disk. Note that because of the random orientation of the momentum kick along the direction $\boldsymbol{n}$, the expectation values of momentum and angular momentum remain unchanged. While the momentum is not strictly balanced when a single particle is put into the wind, it is hence statistically conserved. Also, the expected average increase of the specific kinetic energy of a particle that enters the wind is given by $v_w^2/2$, as desired.

An interesting problem arises because of the finite thickness of a star-forming region. A real wind plausibly originates from a region close to the surface of a star-forming disk, allowing it to leave without greatly impacting ongoing star formation. In the simple model developed here, we do not try to restrict wind formation to a surface layer. Instead, we allow all the SPH particles in the star-forming region to enter the wind if chosen by the probabilistic criterion. However, wind particles from inner parts of star-forming disks would normally be stopped again by other particles in the dense disk, resulting in rapid dissipation and thermalisation of the kinetic energy. In addition, the momentum input would lead to a strong perturbation and, in extreme cases, to a disruption of the disk. This is in disagreement with our assumption that the wind can escape from the dense, star-forming phase without directly affecting it. Only outside the disk, would gasdynamical interactions within the halo stop the wind. To allow such behaviour, we "decouple" a spawned wind particle for a brief time from hydrodynamic interactions, i.e. it neither exerts nor receives hydrodynamic forces during this period. The particle is however included in the computation of the gas density, and for gravity. The full hydrodynamic interactions are enabled again once the density of the particle has fallen to $0.1\,\rho_{\rm th}$, or once a time of
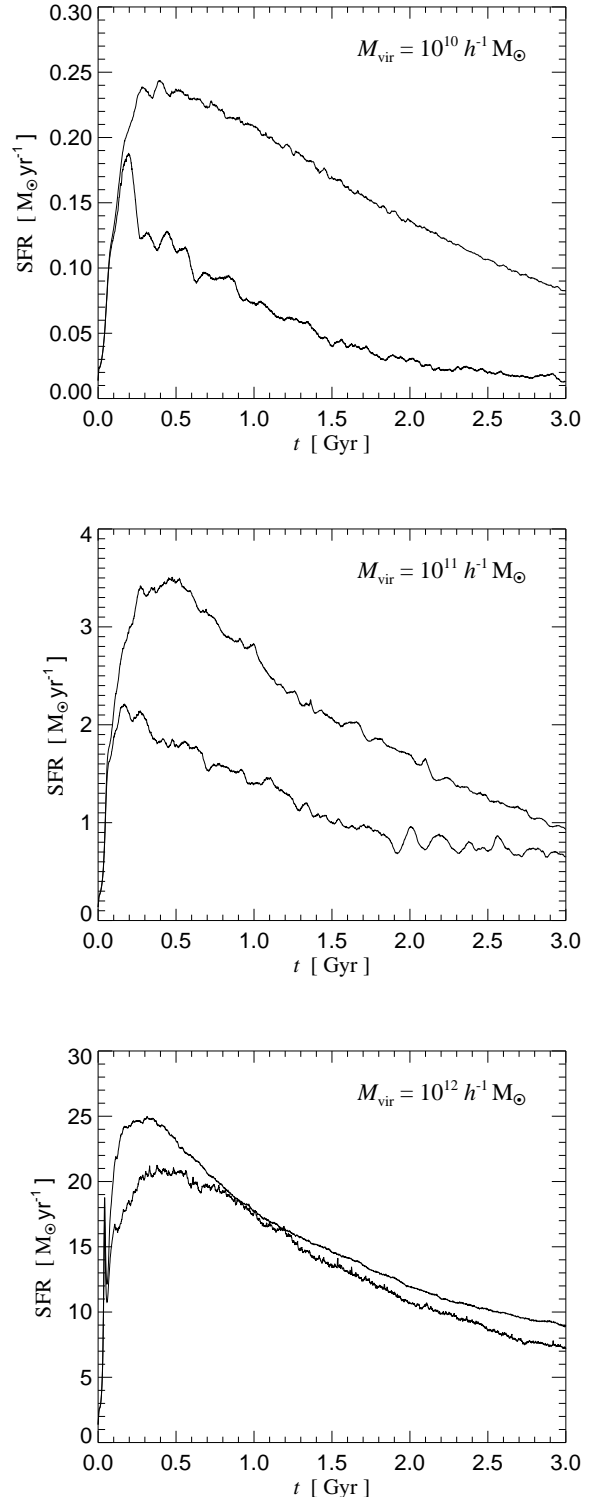

Figure 4. Star formation rates in simulations of disks growing within haloes of different masses, with or without the inclusion of a wind. From top to bottom, the panels show results for haloes of differing total mass: $M_{\rm vir} = 10^{10}\,h^{-1}{\rm M}_\odot$, $10^{11}\,h^{-1}{\rm M}_\odot$, and $10^{12}\,h^{-1}{\rm M}_\odot$, respectively. The inclusion of winds always leads to a net suppression of star formation and hence to a lower curve, but the importance of this effect is a strong function of halo mass.

$\Delta t = 50\,\mathrm{Myr}$ has elapsed, whichever happens earlier. This allows the wind particle to travel "freely" up to a few kpc until it has left the dense star-forming phase. In this way, we can mimic quite well the strong, but quiescent mass-loss from a star-forming region. We have checked that the strength of the wind and the efficiency of wind escape are insensitive to the detailed values chosen for the parameters of this decoupling prescription.

6 TESTS AND RESULTS

The feedback model discussed above has widespread implications for cosmological simulations, influencing nearly all predicted properties of galaxy populations. However, it is beyond the scope of this paper to fully investigate all these consequences in detail. Rather, we focus here on the methodology of the modelling technique. The simulations we present below were selected as test cases to allow us to validate our approach, and to give us insight into key effects of the feedback model in a cosmological context.

More specifically, we focus on two small sets of simulations, one designed to study the problem of disk formation in a highly idealised situation, and the other selected as a full-blown, yet rather small cosmological simulation of structure formation. Results of modelling with higher dynamic range will be presented in due course.

6.1 Isolated spiral galaxies

Currently, simulations of cosmic structure formation still fail to match observed properties of spiral galaxies, although some progress has been achieved recently using improved feedback prescriptions (e.g. Sommer-Larsen et al., 2002). One cause of the difficulty has been that collapsed gas loses too much angular momentum to the dark matter, so that disks are too compact when compared with observations. On the other hand, the spin distribution of dark matter haloes is well understood both analytically and numerically. Simple analytic models indicate that disk sizes in such haloes should match the observed distribution, provided that baryons conserve most of their specific angular momentum during collapse (Mo et al., 1998; van den Bosch et al., 2001; van den Bosch, 2001; van den Bosch et al., 2002).

In our tests here, we will not be concerned with these issues directly. Instead, we examine the inside-out formation of a disk galaxy under idealised settings which allows us to cleanly study the properties of our self-regulated model for star formation, with or without winds. To this end, we consider a series of simulations which effectively follow the Fall & Efstathiou (1980) picture of the formation of a disk galaxy. We set up an NFW-halo (Navarro et al., 1996, 1997) in isolation, with the dark matter and gas initially in virial equilibrium. When evolved in time using adiabatic gas physics, our initial conditions are nearly stable, showing only negligible secular evolution over a Hubble time. However, when the gas is allowed to cool radiatively, the gas in the center of the halo quickly loses its pressure support and settles into a rotationally supported disk that grows from inside out, with a size that depends on the initial angular momentum of the gas. Note that due to the axisymmetric set-up we have cho-

sen, angular momentum transport between the gas and the dark matter is essentially absent in these simulations.

For definiteness, we have chosen a halo of mass $M_{\mathrm{vir}} = 10^{12}\,h^{-1}\mathrm{M}_\odot$, with 10% of the mass being in baryonic form. The initial angular momentum J of the halo can be described in terms of the spin parameter $\lambda = J|E|^{1/2}/(GM_{\mathrm{vir}}^{5/2})$, for which we adopt a value $\lambda = 0.1$ to produce a large disk. The relative distribution of angular momentum within the halo was chosen under the assumption that the specific angular momenta $j(r)$ of spherical shells are all aligned, and that their magnitude is given by the fitting formula

$$j(r) = j_{\max}\left(\frac{M(r)}{M_{\mathrm{vir}}}\right)^s \qquad (43)$$

of Bullock et al. (2001). Within each shell, we distribute the angular momentum as if the shell were in solid body rotation. For $s = 1$, the choice we adopt here, this implies that in the xy-plane, the initial azimuthal streaming velocity is proportional to the circular velocity squared. We have also simulated haloes with masses of $10^{11}\,h^{-1}\mathrm{M}_\odot$, and $10^{10}\,h^{-1}\mathrm{M}_\odot$. They are simply scaled down versions of the $10^{12}\,h^{-1}\mathrm{M}_\odot$ halo, differing by factors of 10 in mass, and by $10^{1/3} \simeq 2.15$ in length and velocity scale.

In order to simplify these test simulations further, we have represented the dark matter halo in most of our runs by a static gravitational potential. This neglects the contraction of the halo due to the infall of the gas, but for the purposes of the present analysis this effect is not important. Simulations that include a live dark halo give very similar results, but are more expensive, especially when one wants to reduce the additional particle noise from the dark halo to a negligible level.

For each of the three halo masses, we run simulations with and without a wind. Typically we used 40000 self-gravitating SPH particles in each case, except for a number of resolution tests which we will discuss separately below. The parameters of our multi-phase model were set to our set of fiducial values, i.e. $t_0^\star = 2.1\,\mathrm{Gyr}$, and for the wind sector, $\eta = 2$ and $\chi = 0.25$.

In Figure 4, we show the star formation rates in these simulations as a function of time. In all cases, the rapid initial development of the gas disk is accompanied by an abrupt rise of the star formation rate to a maximum soon after the start of the simulations. Thereafter, the star formation rate declines nearly exponentially for some time, but the decline becomes increasingly slower at later times. In general, the models with winds yield a lower star formation rate at all times, but the magnitude of the suppression is a strong function of halo mass. The $10^{12}\,h^{-1}\mathrm{M}_\odot$ halo forms stars nearly unaffected by a wind, but the $10^{11}\,h^{-1}\mathrm{M}_\odot$ halo and particularly the $10^{10}\,h^{-1}\mathrm{M}_\odot$ halo suffer a strong reduction in their star formation rates.

The cause for these differences between the effects of the wind in haloes of different mass becomes readily apparent when one examines the flow of the gas in more detail. In Figures 5, 6, and 7, we show the time evolution of the velocity field in the xz-plane, which is a slice orthogonal to the gas disk, with the rotation axis along the z-axis. We indicate the gas velocity field with arrows, overlaid on a colour-scale map showing the gas density in the slice.

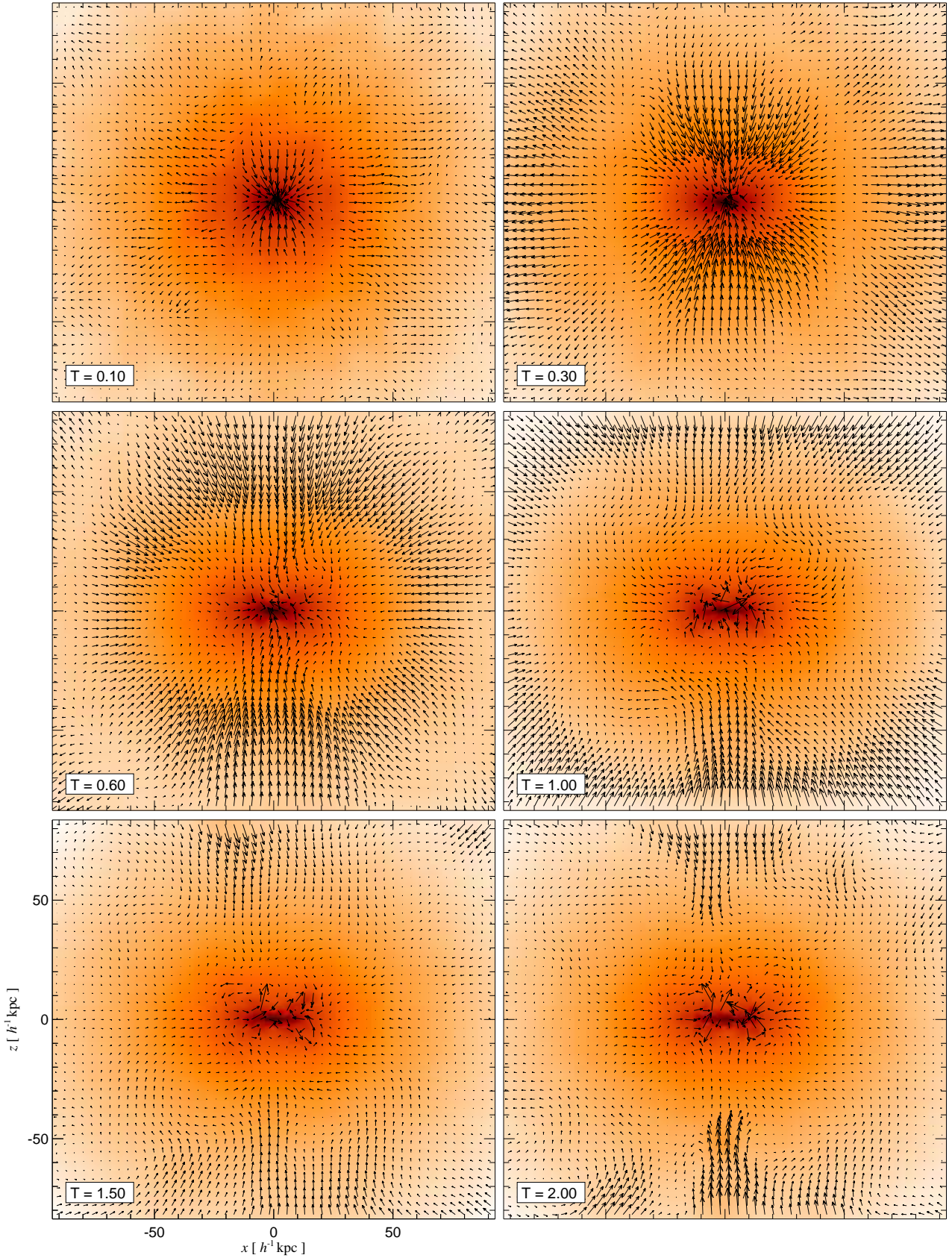For the massive $10^{12}\,h^{-1}\mathrm{M}_\odot$ halo, the wind is never able

Figure 5. Time evolution of the gas flow in a halo of total mass $M_{\mathrm{vir}} = 10^{12}\, h^{-1}\mathrm{M_\odot}$. The velocity field is represented by arrows and the logarithm of the gas density is indicated as a colour-scale. Labels give the elapsed time in $h^{-1}\mathrm{Gyr}$ since the start of the simulation. A wind of speed $242\,\mathrm{km\,s^{-1}}$ is included in this model, but it is stopped already very close to the disk.
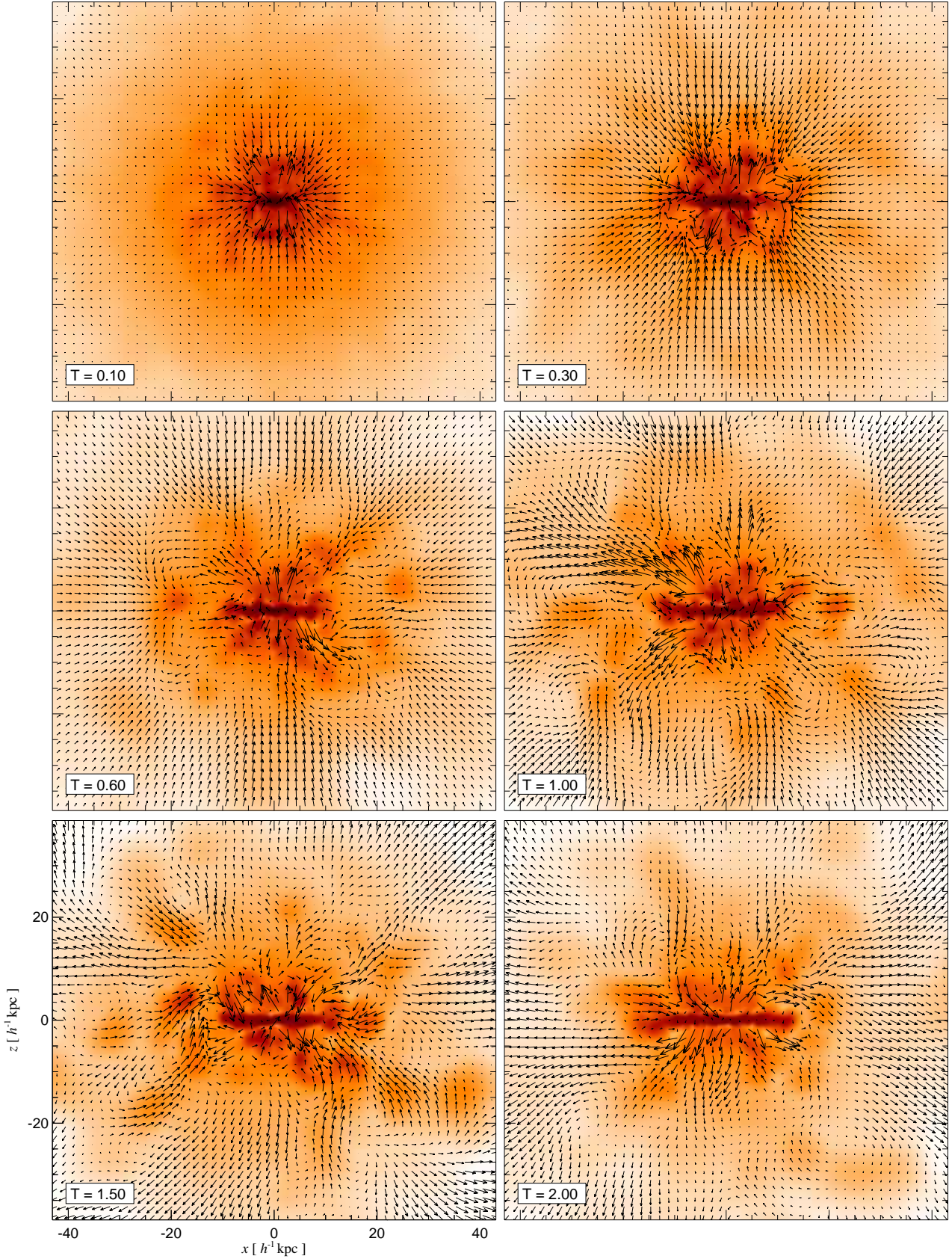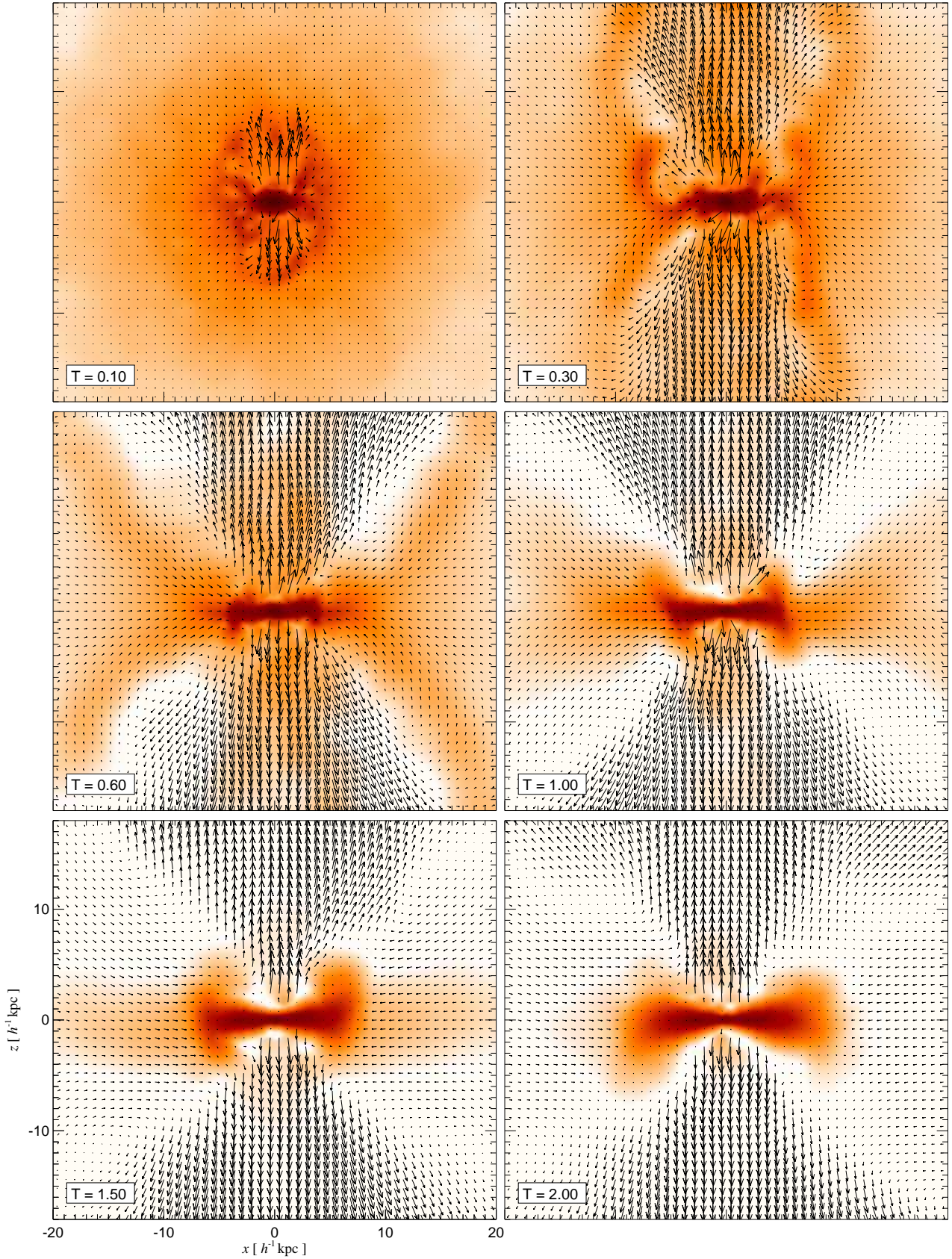
Figure 6. Time evolution of the gas flow in a halo of total mass $M_{\rm vir} = 10^{11}\,h^{-1}{\rm M}_\odot$. The velocity field is represented by arrows and the logarithm of the gas density is indicated as a colour-scale. Labels in each panel give the elapsed time in $h^{-1}{\rm Gyr}$ since the start of the simulation. A wind of speed $242\,{\rm km\,s^{-1}}$ is included in this model, somewhat slower than the escape speed of $v_{\rm esc} \simeq 280\,{\rm km\,s^{-1}}$ from this halo. As a result, gas escapes to substantial heights in the halo, but falls back later onto the disk in a galactic "fountain".

Figure 7. Time evolution of the gas flow in a halo of total mass $M_{\rm vir} = 10^{10} \, h^{-1} {\rm M}_\odot$. The velocity field is represented by arrows and the logarithm of the gas density is indicated as a colour-scale. Labels in each panel give the elapsed time in $h^{-1}{\rm Gyr}$ since the start of the simulation. A wind of speed $242 \, {\rm km \, s^{-1}}$ is included in this model, considerably higher than the escape speed of $v_{\rm esc} \simeq 130 \, {\rm km \, s^{-1}}$ from this halo. As a result, a galactic super-wind develops which blows out of the galaxy, entraining a significant fraction of the gas from the halo.
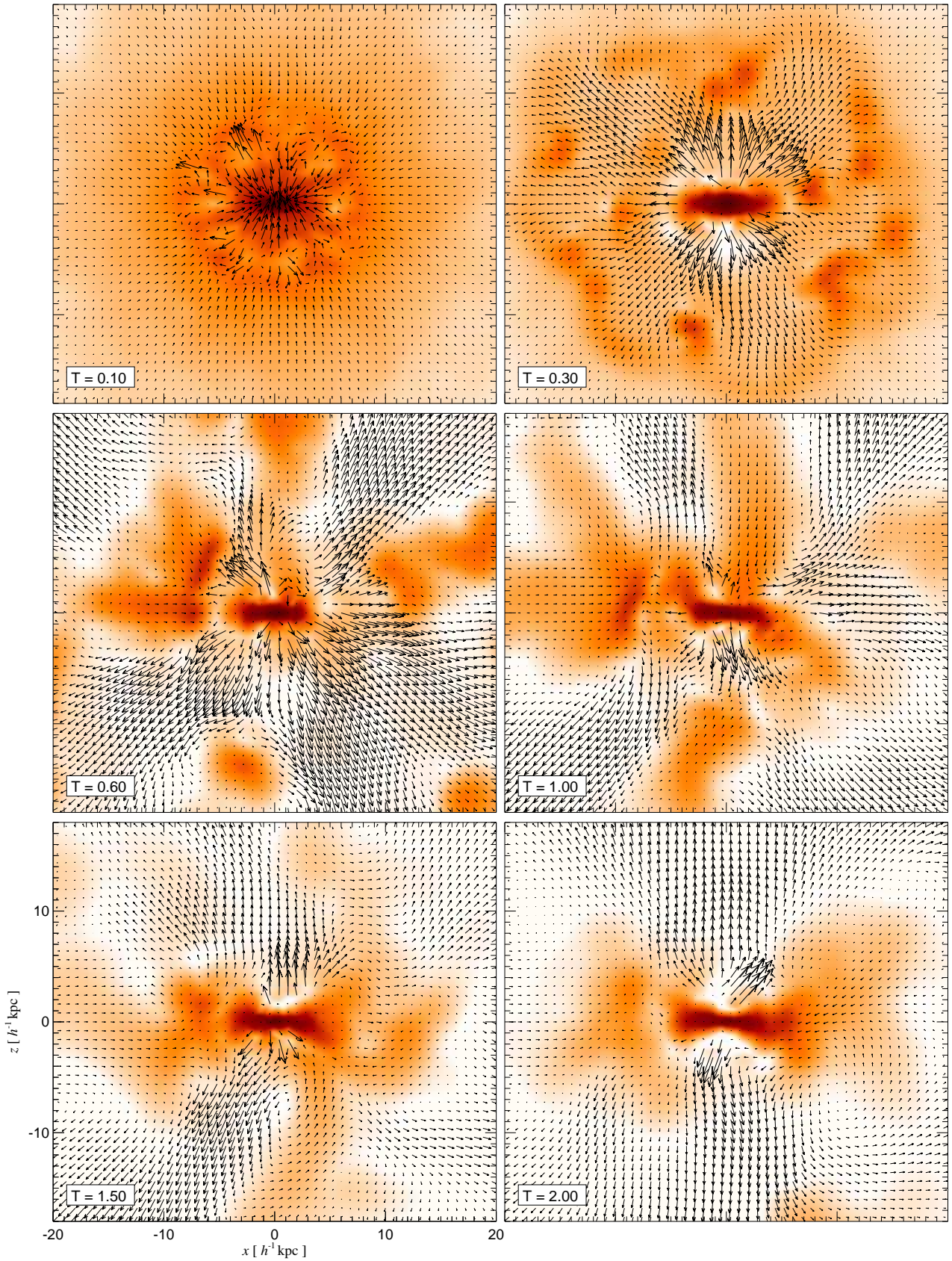
Figure 8. The same as Figure 7, except that the simulation included isotropic winds instead of explicitly modelling an outflow that is preferentially oriented along the rotation axis of the disk. A bipolar outflow pattern orthogonal to the disk still develops for the isotropic wind due to the dense disk that forms in the xy-plane, and due to the non-isotropic inflow pattern. Overall, the gas flow is considerably less ordered in this case, but it is qualitatively still quite similar to the model with axial winds.
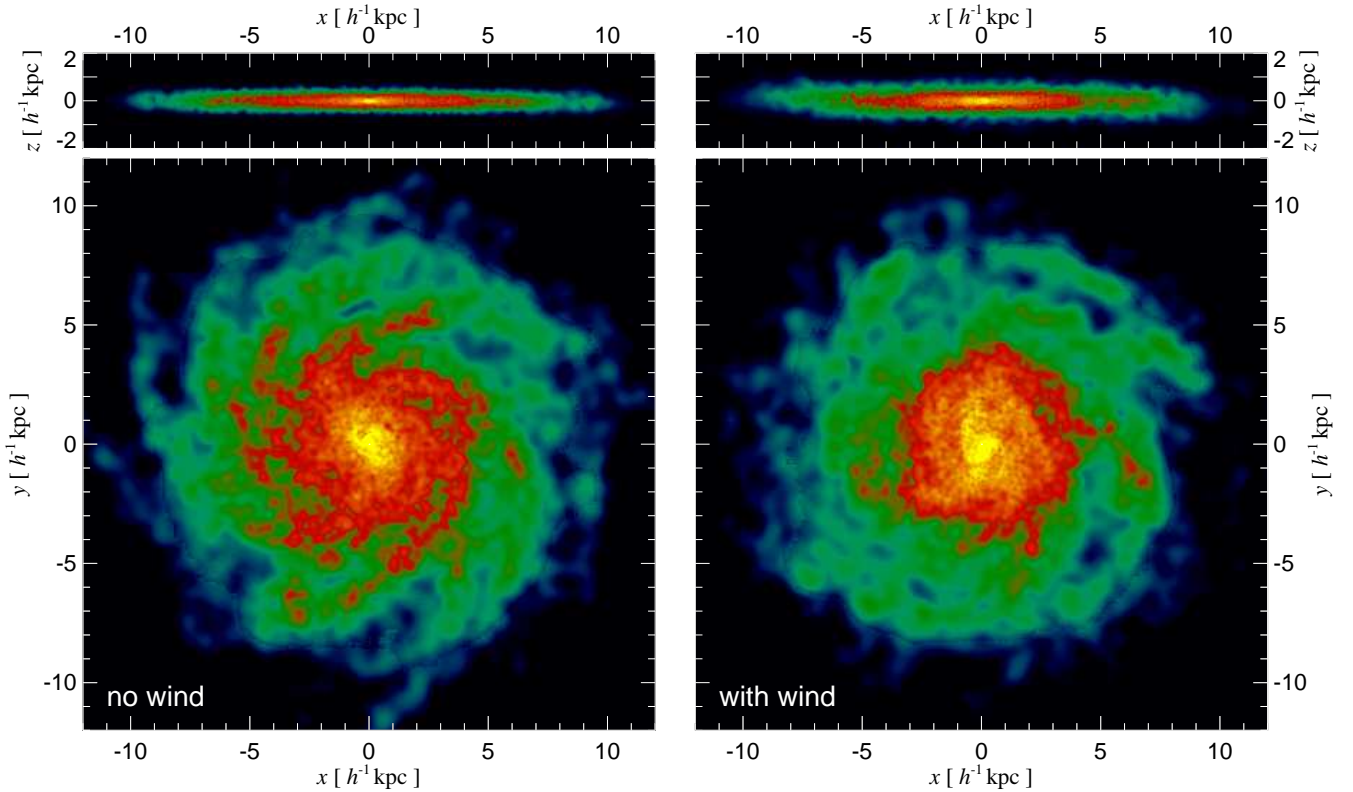
Figure 9. Stellar disk that formed after 3 Gyr in a halo of mass $M_{\rm vir} = 10^{12}\,h^{-1}{\rm M}_\odot$, seen both face on and edge on. On the left, the simulation does not include winds, on the right it does. The colour-contours in the pictures have been set such that they contain roughly the same fraction of the total light in each case.

to propagate very far from the star-forming disk. Instead, any ejected material is quickly stopped by the ram pressure of ambient gas, and, even more important, by the strength of the gravitational force field. Note that the wind speed of $242\,{\rm km\,s}^{-1}$ is comparable to the circular velocity of this halo, but it is still much smaller than the halo's escape velocity.

However, the evolution is already somewhat different in the $10^{11}\,h^{-1}{\rm M}_\odot$ halo, which is shown in Figure 6. In this case, the wind is still not energetic enough to unbind material from the halo, which has an escape velocity of $v_{\rm esc} \simeq 280\,{\rm km\,s}^{-1}$. However, ejected gas is able to rise to substantial heights in the halo and to displace infalling material, before it eventually falls back to the disk, forming a "galactic fountain" (Shapiro & Field, 1976). This process slows down the processing of gas into stars, and it mixes metals into the halo, which thus becomes gradually enriched.

Finally, if the potential well is shallow enough, the wind can escape from the galaxy entirely. This is the case for the $10^{10}\,h^{-1}{\rm M}_\odot$ halo, as shown in Figure 7. The wind velocity is now substantially larger than the escape velocity of $v_{\rm esc} \simeq 130\,{\rm km\,s}^{-1}$, allowing the wind to "blow out" into the intergalactic medium, where it deposits both metals and its residual kinetic energy. The wind can also entrain some of the halo's gas, thereby further reducing the infall rate onto the star-forming disk. Note that our wind model has been specifically constructed to be "quiescent", i.e. to leave the star-forming ISM intact. The wind does not blow away the ISM entirely, but it instead leads to quiescent mass-loss with strength determined by the star formation rate. This re-

moval of baryons, together with the interception of infalling material, leads to a strong reduction of the star formation rate in low-mass haloes.

In the three wind runs discussed above, "axial" wind formation has been used. In the small-mass galaxy shown in Figure 7, this leads to a highly collimated, bipolar outflow. In Figure 8, we show the same model, but computed with isotropic winds. In this case, a bipolar outflow pattern orthogonal to the disk still develops, but due to the dense disk that forms in the xy-plane and the non-isotropic infall pattern of the gas. Overall, this results in a gas flow that is qualitatively still quite similar to the model with axial winds, and the resulting star formation rate is also very similar. In practice, even in this extreme case of a thin centrifugally supported disk, it makes little difference whether isotropic winds or the axial model are used.

It is also interesting to study the stellar disks that develop in these simulations. In Figure 9, we show the luminosity density of the stellar disk that formed in the two $10^{12}\,h^{-1}{\rm M}_\odot$ simulations after a time of 3 Gyr. As expected, a thin stellar disk has grown. Interestingly, the disk morphology appears nearly unaffected by whether or not a wind is included. In both cases, the disks are quite smooth, as are the gaseous layers that form the stars. This is a result of the pressurisation of the gas in our multi-phase model. Note that if the gas was treated as a single-phase medium, it would essentially behave as an isothermal gas at temperature 10^4 K. The disk would then be rather unstable to gravitational per-
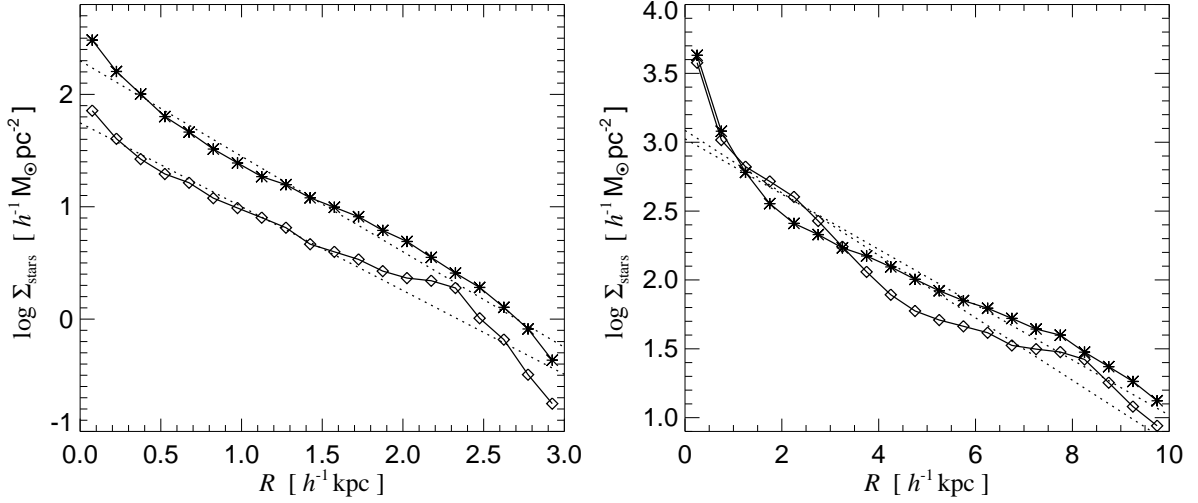
Figure 10. Radial surface brightness profiles for disks that formed in isolated haloes after 3 Gyr. On the left, we show results for a halo of total mass $10^{10}\,h^{-1}\mathrm{M}_\odot$, both for a run without winds (stars) and one with winds (diamonds). The dotted lines are exponential profiles, fitted under the constraint that they give the same total light as the entire simulated disk. The exponential scale lengths of the disks are 0.51 and $0.58\,h^{-1}$kpc, respectively. On the right, the same results are shown for a halo of total mass $10^{12}\,h^{-1}\mathrm{M}_\odot$, with the exponential fits giving scale lengths 2.1 and $1.9\,h^{-1}$kpc, respectively.
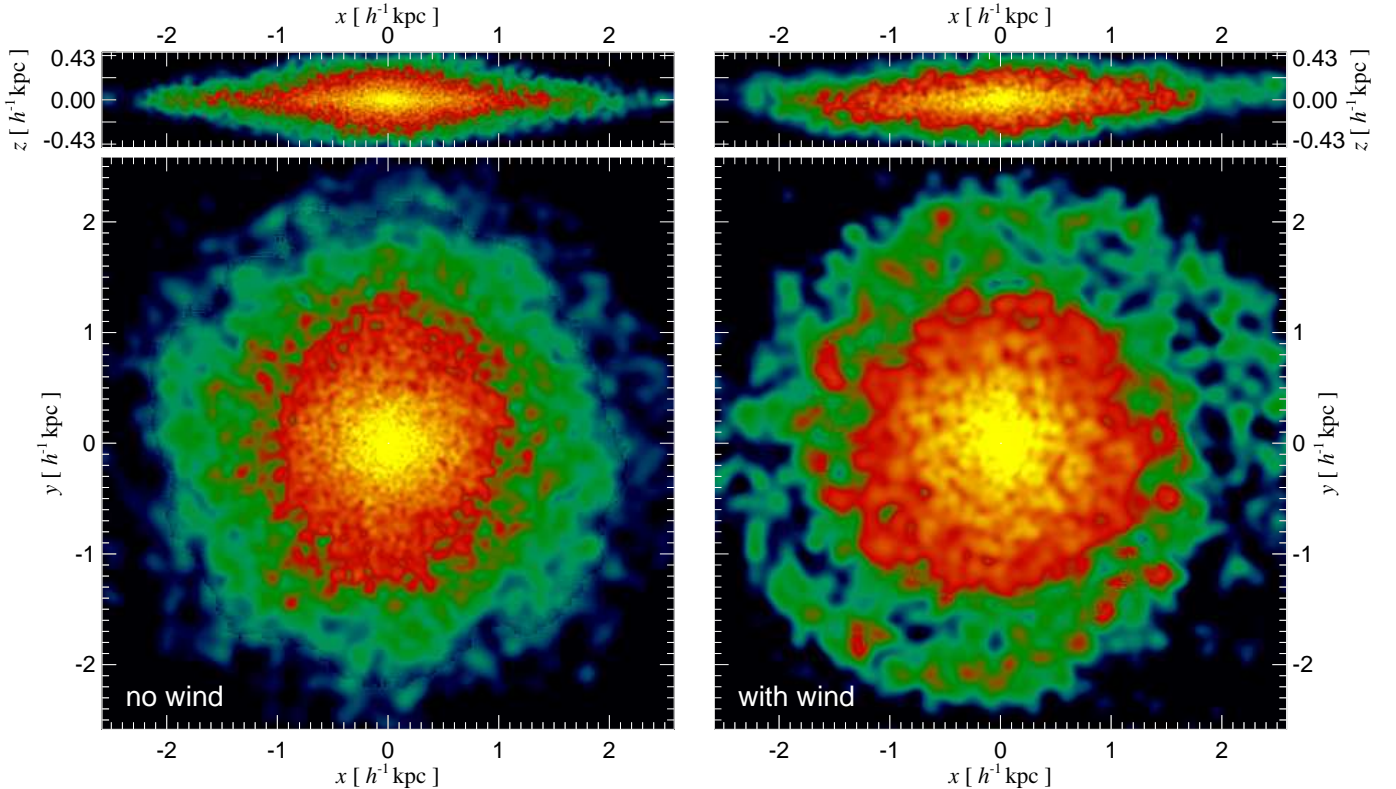
Figure 11. The stellar disk that formed after 3 Gyr in a halo of mass $M_{\mathrm{vir}} = 10^{10}\,h^{-1}\mathrm{M}_\odot$, seen both face on and edge on. On the left, the simulation does not include winds, on the right it does. The colour-contours in the pictures have been set such that they contain roughly the same fraction of the total light in each case. Note that the the morphology of the two disks appears similar, but the model that includes the wind has only 36% of the luminosity of the run that does not.
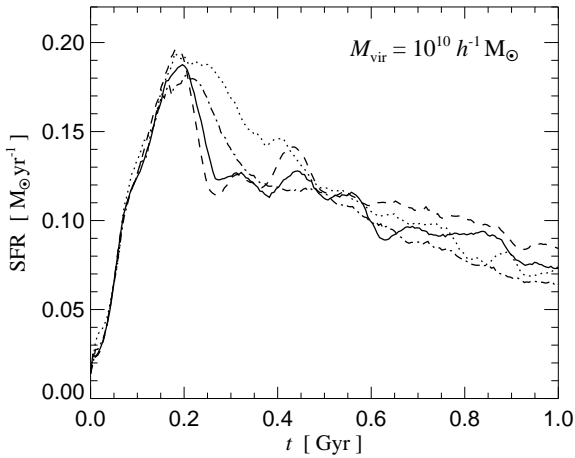
Figure 12. Convergence study of the star formation rate in four runs that differ in total by a factor 64 in mass resolution. The simulations include winds and describe the formation of a disk in a $10^{10}\,h^{-1}\mathrm{M}_\odot$ halo. We show results for simulations with 40000 (solid), 160000 (dashed), 10000 (dot-dashed), and 2500 (dotted) particles. The gravitational softening used in the simulations was varied in proportion to the cube root of the mass resolution, ranging from 0.03 to $0.12\,h^{-1}\mathrm{kpc}$.

turbations and would be bound to quickly break up into many lumps.

The radial surface brightness profiles of the disks are shown in Figure 10. In the main body of the galaxy, the profile is reasonably well fitted by an exponential, but there is a clear deviation towards higher luminosities in the centre. This is probably a consequence of the initial angular momentum distribution that we adopted. For similar assumptions about the distribution of initial angular momentum, analytic computations of disk formation predict a similar effect (van den Bosch, 2001).

Figure 10 also shows how the influence of the wind depends on halo mass. While the stellar profile for the $10^{12}\,h^{-1}\mathrm{M}_\odot$ halo is nearly unaffected by the winds, the small $10^{10}\,h^{-1}\mathrm{M}_\odot$ halo suffers a reduction in its surface brightness by nearly a factor of 3. However, the radial scale lengths are essentially unaffected, as are the disk morphologies. The latter can be seen in more detail in Figure 11, where we show the projected stellar mass densities for the low-mass halo. In comparison to Fig. 9, it is clear that the ratio of disk scale height to radial scale length is larger for the smaller halo. This is a direct consequence of the effective equation of state of the multi-phase medium. The effective pressure stabilises the gas disks vertically against gravity, but in doing so it imposes a certain scale, i.e. the scale height depends only weakly on surface mass density and does not fall below $\sim 150\,\mathrm{pc}$ in our model.

Finally, we briefly examine the sensitivity of our numerical results to the mass resolution employed. This is a particularly important test, not only to assess numerical convergence in general, but also for establishing the suitability of the method for cosmological simulations of structure formation. In such calculations, haloes of different mass are invariably resolved with a different number of particles. If

the numerical results for star formation and feedback depend sensitively on mass resolution, differential resolution effects would be introduced that could severely compromise an interpretation of the results. Note that this also implies that the free parameters of any feedback model that behaves well in this respect should be independent of resolution.

By construction, we expect the model described in this paper to meet these requirements, primarily because the feedback and star formation schemes are formulated in terms of an effective subresolution model which does not require an explicit reference to the particle formalism. We test this contention by repeating the wind-simulation of the $10^{10}\,h^{-1}\mathrm{M}_\odot$ halo at a number of different mass resolutions, both with smaller and larger particle numbers than the 40000 used above. In particular, we selected mass resolutions of 2500, 10000, and 160000 particles, thereby obtaining a series of runs that stretches a dynamic range of 64 in mass resolution. We also varied the 3D spatial resolution (i.e. the gravitational softening length) in proportion to the cube root of the mass resolution, as it is typically done in cosmological simulations of structure formation. In Figure 12, we compare the star formation rates measured as a function of time in these simulations. Reassuringly, the agreement is rather good between all four runs, confirming that the model outlined above is numerically well posed. The formulation in terms of an effective sub-resolution model has a well-specified continuum limit, and we do not expect the results of this test to change even when the resolution is increased indefinitely. This means, however, that much higher resolution would not begin to eventually resolve the "true" spatial structure of the ISM – in order to do this faithfully, the effective model would have to be dropped.

6.2 Cosmic star formation history

We now employ our multi-phase model in full cosmological simulations of structure formation. In this paper, we restrict ourselves to highlighting some of the main consequences of the model with respect to the overall star formation rate and the metal enrichment of the IGM. For these purposes, it is sufficient to consider moderate-sized simulations of a relatively small volume. In particular, we work with 2×50^3 dark matter and SPH particles in a box of length $11.3\,h^{-1}\mathrm{Mpc}$ per side. This gives a mass resolution of $m_{\mathrm{gas}} = 1.28\times10^8\,h^{-1}\mathrm{M}_\odot$ in the gas and $m_{\mathrm{dm}} = 8.33\times10^8\,h^{-1}\mathrm{M}_\odot$ in the dark matter, for a canonical ΛCDM cosmology with parameters $\Omega_0 = 0.3$, $\Omega_\Lambda = 0.7$, $\Omega_b = 0.04$, $h = 0.67$, and $\sigma_8 = 0.9$. We have run several of these simulations for different parameter choices, and in addition one run where we stepped up the mass resolution by a factor of eight to 2×100^3 particles.

Note that the simulation volume in these runs is much too small to be representative of the universe as a whole, and in fact, the largest modes in the box become non-linear by $z = 0$. Nevertheless, the simulations suffice to identify the systematic effects that arise from our feedback schemes, and from the winds, in particular. However, it should be kept in mind that simulations of larger size with comparable or better mass resolution are required to arrive at quantitatively accurate results for cosmological expectation values such as the mean luminosity density.

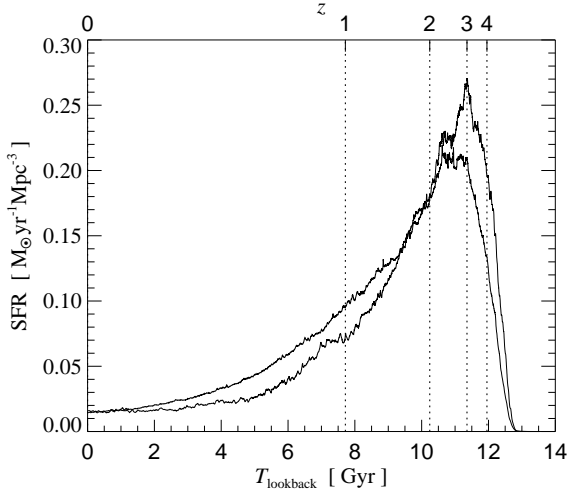In Figure 13, we show the cosmic star formation history

Figure 13. Comoving star formation history of two small cosmological simulations, using the hybrid multi-phase model without winds for star formation timescales $t_0^\star = 1\,\mathrm{Gyr}$ and $t_0^\star = 4.2\,\mathrm{Gyr}$, respectively. For a smaller value of $t_0^\star$, the peak of the star formation rate moves to higher redshift, and the decline towards the present epoch proceeds faster. However, the integrated mass of stars that forms up to $z = 0$ is insensitive to $t_0^\star$: the short-timescale model turns 18.2% of the baryons into stars, the long-timescale model 18.4%.

Figure 14. Evolution of the cosmic star formation density for different simulations. The solid line gives the star formation rate per comoving volume for our fiducial 2×50^3 simulation, with parameters $t_0^\star = 2.1\,\mathrm{Gyr}$, $\eta = 2$, and $\chi = 0.25$. The dot-dashed line is for the same model, but at a higher resolution of 2×100^3. The dashed line shows a model with a much more energetic wind, specified by $\eta = 0.5$ and $\chi = 1$, while the dotted line shows the result for a run without winds.

for two of our wind-less 2×50^3 simulations, differing only in the value adopted for the star formation timescale $t_0^\star$. While a larger value of this parameter shifts star formation towards later times, the integrated star formation history is insensitive to the value of $t_0^\star$. Ultimately, if only the quiescent model of star formation is considered, the mass of stars that forms is approximately given by the amount of baryons that can cool, because the gas consumption timescale is significantly shorter than the age of the universe. It is, however, well known that cooling alone is quite efficient (e.g. White & Rees, 1978; White & Frenk, 1991; Katz & White, 1993; Pearce et al., 1999; Lewis et al., 2000; Davé et al., 2001; Balogh et al., 2001; Springel & Hernquist, 2002a), leading to a collapse fraction well in excess of observational bounds on the amount of baryons in stars and cold gas. For example, Fukugita et al. (1998) use optical data to constrain the fraction of baryons in the form of cold gas or stars to be in the range of 6.2% to 16.7%. Balogh et al. (2001) derive an even lower value of about 5%, based on the K-band luminosity function (Cole et al., 2001), which should in principle provide a more robust estimate due to the relatively weak dependence of the K-band mass-to-light ratio on star formation history. However, some uncertainty arises from the adopted IMF; as Cole et al. (2001) discuss, an estimate of the mass fraction in stars higher by about a factor of 2 is obtained if a Salpeter IMF (1955) instead of a Kennicutt (1983) IMF is assumed. Note that there are also tight limits on the amount of gas in neutral and molecular form, implying that they together can only account for at most 10% of the mass bound in stars. Hence, most of the condensed gas should in fact be bound in stars, and there is not much room to "hide" gas that has cooled.

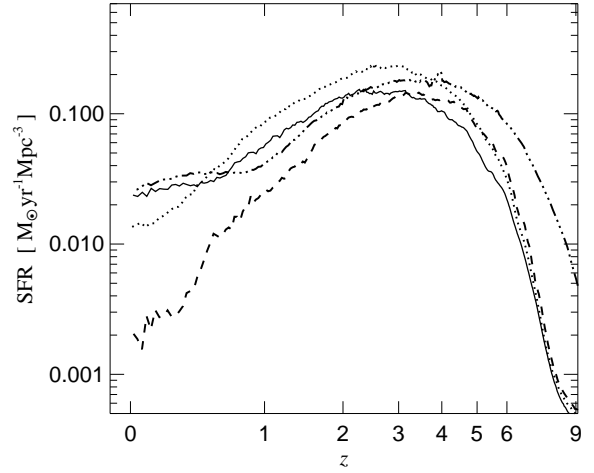The discrepancy between the high efficiency of cooling

and the low abundance of stars suggests that any feedback model lacking a mechanism for returning baryons from the condensed phase into the extended halo or IGM will be unable to account for the observations. For example, in the no-wind runs shown in Fig. 13, more than 18.2% of the baryons are locked up in stars, which is already above current observational constraints, even though this number represents an underestimate due to the limited resolution of these simulations, and it does not yet include the dense, neutral gas remaining in the simulation.

However, winds are able to significantly affect the cosmic star formation history. In Figure 14, we show simulation results for the comoving star formation density as a function of redshift for different wind strengths. The dotted line shows a 2×50^3 run using our fiducial set of parameters and the quiescent model of star formation without winds. The solid line is the same model, but this time including winds with a strength specified by $\eta = 2$ and $\chi = 0.25$, i.e. star-forming regions blow a wind with speed $242\,\mathrm{km\,s^{-1}}$ at a mass-loss rate equal to twice the star formation rate. This reduces the integrated star formation rate such that 13.5% of the baryons become bound in stars, providing a better match to direct observational constraints of the cosmic luminosity density, although perhaps still being uncomfortably high.

Faster winds can escape from bigger haloes and provide larger heating to the surrounding IGM. This can make them more effective in reducing subsequent star formation, even if the mass-loss rate is smaller. For example, the dashed line in Fig. 14 shows a rather extreme wind model, with $\eta = 0.5$ and $\chi = 1$. The wind has thus an initial speed of $968\,\mathrm{km\,s^{-1}}$, but a mass-loss rate four times smaller than in our fiducial model. This energetic wind leads to substantial heating of

the IGM, and reduces the star formation rate considerably, such that this model turns only 8% of its baryons into stars.

Finally, we also show the result for a 2×100^3 simulation of our fiducial model. Here, the star formation rate is substantially larger at high redshift. This is expected because the improved resolution now allows much more of the star formation to be seen in low-mass objects that begin to form abundantly at high redshift. It is thus clear that much better resolution than was used in the 2×50^3 runs is required to obtain converged results in the high-redshift regime. However, this is not necessarily the case for the integrated star formation rate. Since the elapsed time is rather small at high redshift, the amount of stellar material formed then is small compared to the total, despite the large star formation rates. Therefore, the 2×100^3 run produces only moderately more stars by $z = 0$; the fraction of baryons is 14.8%, up from 13.5% for the corresponding 2×50^3 run. Note that the slight upturn seen in the 2×50^3 and 2×100^3 runs with slow winds at redshifts below $\simeq 0.5$ is due to the small box size of these simulations, which do not allow a proper sampling of the halo mass function at low redshift, where in fact the fundamental modes of the boxes already become non-linear. In particular, the star formation rate begins to be dominated by the few most massive halos in the box, and they are able to reaccrete at low redshift some of the gas ejected by winds out of their progenitor halos. If larger cosmological volumes are simulated, such biases in the estimated mean of the cosmic star formation density can be avoided (Springel & Hernquist, 2002b).

6.3   Metal enrichment of the IGM

As we discussed in Section 4, galactic winds may be of crucial importance for the transport of metals into the IGM, where they have been observed in absorption line systems down to very low column densities. In Figure 15, we show the mean metallicity of the gas as a function of baryonic overdensity in our cosmological simulations. We give results at redshifts $z = 4$, $z = 2.33$, and $z = 0$, for runs carried out with our fiducial parameters, both with and without winds.

It is evident that in the simulation without winds, metals are nearly confined to gas with overdensities $\delta > 10$. At redshift $z = 0$, such gas reaches a metallicity of about $10^{-4} Z_\odot$, where $Z_\odot$ is the solar metallicity. However, at redshifts higher than $z > 2.3$ even gas at overdensities 100 is well below $10^{-4} Z_\odot$, and thus falls significantly short of the metallicities that are observed in the Ly-α forest at these redshifts, as indicated by the shaded region (following Aguirre et al., 2001a). Recall that in our self-regulated model for star formation, stars begin to form only at high physical densities, corresponding to baryonic overdensities of about $\sim 10^6$ at $z = 0$. If winds are not included, only dynamical stripping may bring metal-enriched gas from the ISM to the lower density environments. The results of Fig. 15 suggest that these processes are not efficient enough to explain the enrichment of the IGM.

However, including winds changes the enrichment pattern significantly, as expected. Our fiducial model enriches the IGM to an interesting metallicity of $Z \simeq 10^{-2.5} Z_\odot$ for the relevant densities. It is thus clear that a wind model like the one discussed here can in principle account for the mean metallicity of the IGM.
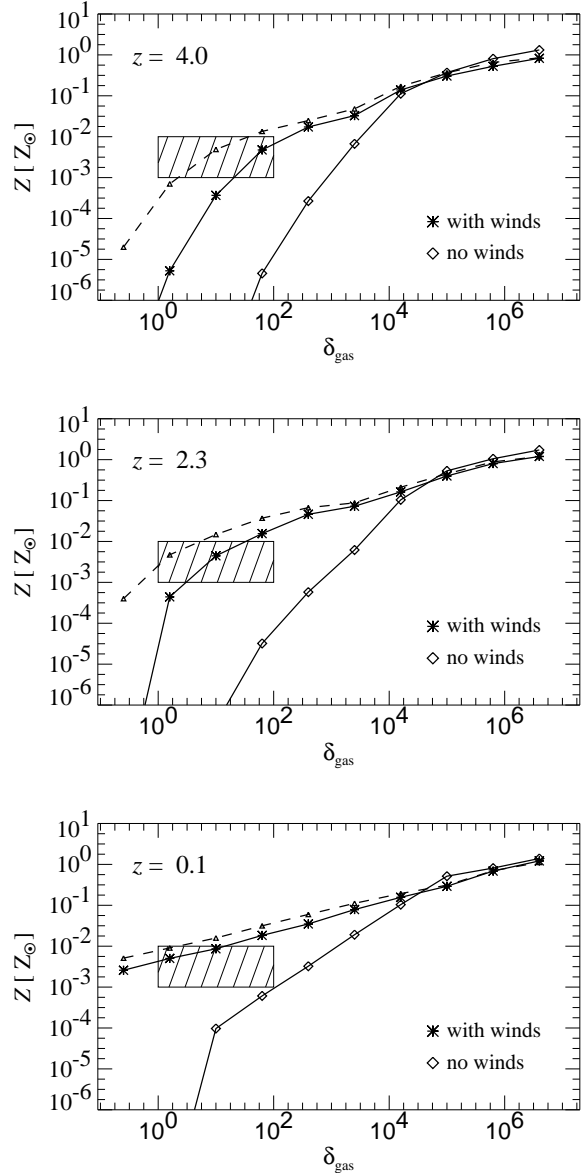

Figure 15. Mean metallicity of the gas as a function of baryonic overdensity. The three panels show results for redshifts $z = 4$, $z = 2.3$, and $z = 0$, both for simulations with and without winds. We follow Aguirre et al. (2001a) and use a shaded region to approximatively indicate the range of metallicities observed in Ly-α absorption line studies at $z \simeq 3$.

Note that the distribution of metals in the gas is highly inhomogeneous. This is seen in Figure 16, where we show projected metallicity maps at redshifts $z = 2.3$ and $z = 0$. The detailed metallicity distribution together with the inhomogeneous heating pattern due to the winds potentially yield signatures in the Ly-α forest that may be very constraining for the enrichment model discussed here. We plan to address this question further in future work. Note that at low velocities, winds will primarily be able to escape from small haloes, pushing the epoch of enrichment of the IGM to high redshift, when these haloes form abundantly, and
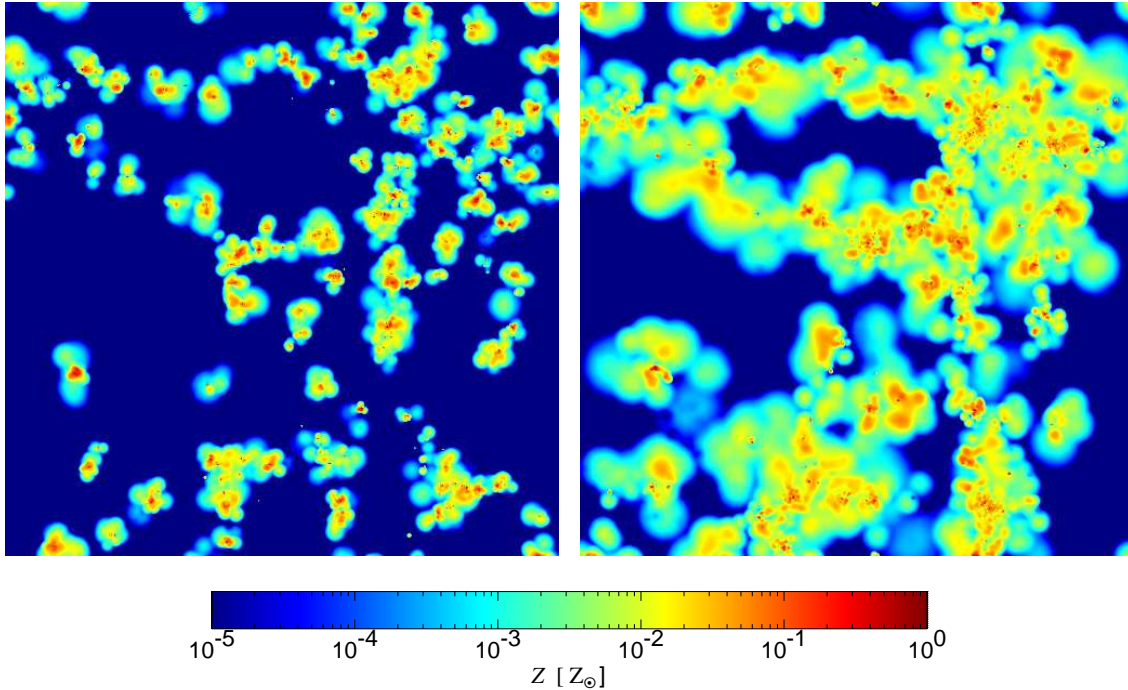
Figure 16. Projected mean metallicity of the gas in a 2×50^3 simulation that includes galactic winds. The map is $11.3\,h^{-1}$Mpc on a side and shows the full simulation box in projection at redshift $z = 2.3$ (left) and $z = 0$ (right). The mean metallicity of the gas is indicated by a logarithmic colour-scale.

when the winds can propagate relatively far because of the small scale-size of the universe at the epoch of ejection.

7 DISCUSSION

We have presented a new model for the treatment of star formation and feedback in cosmological simulations of galaxy formation. Our approach leads to the establishment of a tight self-regulation cycle for star formation which is based on a rough, yet physically motivated model of the ISM. A crucial ingredient of the model is the assumed multi-phase structure of the ISM. At high density, much of the interstellar material becomes bound in cold clouds, becoming sites for star formation. The density of the ambient phase is lowered accordingly, which also reduces its radiative losses and allows it to be heated by supernovae to a temperature high enough to provide some pressure support for the ISM. The stabilising effect of this pressure counteracts star formation and, together with the cloud formation/evaporation cycle, leads to self-regulation. Due to the nature of the approximations made, it is clear that our model is still phenomenological to a large degree. In principle, however, the physical approximations we used can be refined in the future, thereby improving the faithfulness of the model.

The star formation timescale in the quiescent mode of star formation can be directly determined from observations of local disk galaxies. If this normalisation is adopted, we find that cosmological simulations nevertheless lead to an overproduction of stars. We have invoked galactic winds as a heuristic extension of our model to remedy this problem. While there is mounting observational evidence for the existence of such winds, they are introduced in our model in a phenomenological manner. However, winds clearly have a range of highly interesting consequences. They reduce the global efficiency of star formation, and this suppression is particularly strong in low-mass haloes, thereby helping to explain the observed "low" values of the luminosity density. Winds are also capable of accounting for the enrichment of the low-density IGM with metals, and they may be crucial to understanding the metal distribution in the intra-cluster gas of clusters of galaxies.

Another important property of our technique is that it is numerically well posed in the sense that the parameters of the model can be determined directly based on physical arguments or observational input, and need not to be changed when the mass resolution is varied. The use of the sub-resolution technique introduces a well-specified continuum limit in the hydrodynamic equations, despite the inclusion of cooling. Unlike in standard single-phase simulations, an unphysical collapse of gas to a scale set by the resolution limit of the simulation is thus prevented. Combined with improved formulations of SPH (Springel & Hernquist, 2002a) this makes it much easier to reach numerical convergence even under conditions of only moderate resolution.

It will thus be interesting to study the predictions of our model in more detail. As first steps, we have already carried out a detailed analysis of the predictions of the model for the cosmic star formation history in the ΛCDM cosmology (Springel & Hernquist, 2002b), and we analysed the impact of cooling, star formation, and winds on secondary anisotropies of the cosmic microwave background (White et al., 2002). In these studies, a new comprehensive set of simulations that included strong galactic winds was used. We plan to extend our analysis of these simulations in future work.

ACKNOWLEDGEMENTS

REFERENCES

Aguirre A., 1999a, ApJ, 512, L19

Aguirre A., 1999b, ApJ, 525, 583

Aguirre A., Hernquist L., Katz N., Gardner J., Weinberg D., 2001a, ApJ, 556, L11

Aguirre A., Hernquist L., Schaye J., Katz N., Weinberg D., Gardner J., 2001b, ApJ, 561, 521

Aguirre A., Hernquist L., Schaye J., Weinberg D., Katz N., Gardner J., 2001c, ApJ, 560, 599

Ascasibar Y., Yepes G., Gottlöber S., Müller V., 2002, A&A, 387, 396

Balogh M. L., Pearce F. R., Bower R. G., Kay S. T., 2001, MNRAS, 326, 1228

Barnes J. E., 1988, ApJ, 331, 699

Barnes J. E., Hernquist L., 1992, ARA&A, 30, 705

Barnes J. E., Hernquist L. E., 1991, ApJ, 370, L65

Begelmann M. C., McKee C. F., 1990, ApJ, 358, 375

Binney J., Gerhard O., Silk J., 2001, MNRAS, 321, 471

Bland-Hawthorn J., 1995, Proc. Astron. Soc. Australia, 12, 190

Blanton M., Cen R., Ostriker J. P., Strauss M., 1999, ApJ, 522, 590

Bryan G. L., Cen R., Norman M. L., Ostriker J. P., Stone J. M., 1994, ApJ, 428, 405

Bryan G. L., Norman M. L., 1998, ApJ, 495, 80

Bullock J. S., Dekel A., Kolatt T. S., et al., 2001, ApJ, 555, 240

Cen R., Miralda-Escudé J., Ostriker J. P., Rauch M. J., 1994, ApJ, 437, L9

Cen R., Ostriker J. P., 1993, ApJ, 417, 415

Cen R., Ostriker J. P., 2000, ApJ, 538, 83

Cole S., Aragon-Salamanca A., Frenk C. S., Navarro J. F., Zepf S. E., 1994, MNRAS, 271, 781

Cole S., Norberg P., Baugh C. M., et al., 2001, MNRAS, 326, 255

Dahlem M., Petr M. G., Lehnert M. D., Heckman T. M., Ehle M., 1997, A&A, 320, 731

Davé R., Cen R., Ostriker J. P., et al., 2001, ApJ, 552, 473

Davé R., Hernquist L., Katz N., Weinberg D. H., 1999, ApJ, 511, 521

Efstathiou G., 2000, MNRAS, 317, 697

Elizondo D., Yepes G., Kates R., Klypin A., 1999a, New Astronomy, 4, 101

Elizondo D., Yepes G., Kates R., Müller V., Klypin A., 1999b, ApJ, 515, 525

Evrard A. E., 1988, MNRAS, 235, 911

Evrard A. E., 1990, ApJ, 363, 349

Fall S. M., Efstathiou G., 1980, MNRAS, 193, 189

Field G. B., 1965, ApJ, 142, 531

Field G. B., Goldsmith D. W., Habing H. J., 1969, ApJ, 155, L149

Frye B., Broadhurst T., Benitez N., 2002, ApJ, 568, 558

Fukugita M., Hogan C. J., Peebles P. J. E., 1998, ApJ, 503, 518

Gerritsen J. P. E., Icke V., 1997, A&A, 325, 972

Gnedin N., 1998, MNRAS, 294, 407

Gnedin N., Ostriker J., 1997, ApJ, 486, 581

Haardt F., Madau P., 1996, ApJ, 461, 20

Heckman T. M., Dahlem M., Lehnert M. D., Fabbiano G., Gilmore D., Waller W. H., 1995, ApJ, 448, 98

Heckman T. M., Lehnert M. D., Strickland D. K., Armus L., 2000, ApJS, 129, 493

Hernquist L., 1989, Nature, 340, 687

Hernquist L., 1992, ApJ, 400, 460

Hernquist L., 1993, ApJ, 409, 548

Hernquist L., Katz N., 1989, ApJ, 70, 419

Hernquist L., Katz N., Weinberg D. H., Miralda-Escudé J., 1996, ApJ, 457, L51

Hiotelis N., Voglis N., 1991, A&A, 243, 333

Hultman J., Pharasyn A., 1999, A&A, 347, 769

Katz N., Gunn J. E., 1991, ApJ, 377, 365

Katz N., Hernquist L., Weinberg D. H., 1992, ApJ, 399, L109

Katz N., Hernquist L., Weinberg D. H., 1999, ApJ, 523, 463

Katz N., Weinberg D. H., Hernquist L., 1996, ApJS, 105, 19

Katz N., White S. D. M., 1993, ApJ, 412, 455

Kauffmann G., Colberg J. M., Diaferio A., White S. D. M., 1999a, MNRAS, 303, 188

Kauffmann G., Colberg J. M., Diaferio A., White S. D. M., 1999b, MNRAS, 307, 592

Kauffmann G., Guiderdoni B., White S. D. M., 1994, MNRAS, 267, 981

Kauffmann G., White S. D. M., Guiderdoni B., 1993, MNRAS, 264, 201

Kay S. T., Pearce F. R., Frenk C. S., Jenkins A., 2002, MNRAS, 330, 113

Kennicutt R. C., 1983, ApJ, 272, 54

Kennicutt R. C., 1989, ApJ, 344, 685

Kennicutt R. C., 1998, ApJ, 498, 541

Lacey C., Silk J., 1991, ApJ, 381, 14

Lehnert M. D., Heckman T. M., 1996, ApJ, 462, 651

Lewis G. F., Babul A., Katz N., Quinn T., Hernquist L., Weinberg D. H., 2000, ApJ, 536, 623

Mac Low M.-M., Ferrara A., 1999, ApJ, 513, 142

Madau P., Ferrara A., Rees M. J., 2001, ApJ, 555, 92

Martin C. L., 1999, ApJ, 513, 156

Martin C. L., Kennicutt R. C., 2001, ApJ, 555, 301

McKee C. F., Ostriker J. P., 1977, ApJ, 218, 148

Mihos J. C., Hernquist L., 1994, ApJ, 437, 611

Mihos J. C., Hernquist L., 1996, ApJ, 464, 641

Mo H. J., Mao S., White S. D. M., 1998, MNRAS, 295, 319

Nath B. B., Trentham N., 1997, MNRAS, 291, 505

Navarro J. F., Benz W., 1991, ApJ, 380, 320

Navarro J. F., Frenk C. S., White S. D. M., 1996, ApJ, 462, 563

Navarro J. F., Frenk C. S., White S. D. M., 1997, ApJ, 490, 493

Navarro J. F., Steinmetz M., 1997, ApJ, 478, 13

Navarro J. F., Steinmetz M., 2000, ApJ, 538, 477

Navarro J. F., White S. D. M., 1993, MNRAS, 265, 271

Navarro J. F., White S. D. M., 1994a, MNRAS, 267, 401

Navarro J. F., White S. D. M., 1994b, MNRAS, 267, 401

Pearce F. R., Jenkins A., Frenk C. S., et al., 1999, ApJ, 521, L99

Pearce F. R., Jenkins A., Frenk C. S., et al., 2001, MNRAS, 326, 649

Pettini M., Shapley A. E., Steidel C. C., et al., 2001, ApJ, 554, 981

Pettini M., Steidel C. C., Adelberger K. L., Dickinson M., Giavalisco M., 2000, ApJ, 528, 96

Rownd B. K., Young J. S., 1999, AJ, 118, 670

Salpeter E. E., 1955, ApJ, 121, 161

Scannapieco E., Broadhurst T., 2001a, ApJ, 550, L39

Scannapieco E., Broadhurst T., 2001b, ApJ, 549, 28

Scannapieco E., Ferrara A., Broadhurst T., 2000, ApJ, 536, L11

Scannapieco E., Thacker R. J., Davis M., 2001, ApJ, 557, 605

Shapiro P. R., Field G. B., 1976, ApJ, 205, 762

Sommer-Larsen J., Gelato S., Vedel H., 1999, ApJ, 519, 501

Sommer-Larsen J., Gotz M., Portinari L., 2002, Ap&SS, 281, 519

Springel V., 2000, MNRAS, 312, 859

Springel V., Hernquist L., 2002a, MNRAS, 333, 649

Springel V., Hernquist L., 2002b, preprint, astro-ph/0206395

Springel V., White S. D. M., 1999, MNRAS, 307, 162

Springel V., White S. D. M., Tormen B., Kauffmann G., 2001a, MNRAS, 328, 726

Springel V., Yoshida N., White S. D. M., 2001b, New Astronomy, 6, 79

Steinmetz M., Müller E., 1995, MNRAS, 276, 549

Steinmetz M., Navarro J. F., 1999, ApJ, 513, 555

Thacker R. J., Couchman H. M. P., 2000, ApJ, 545, 728

Thacker R. J., Couchman H. M. P., 2001, ApJ, 555, L17

Thomas P. A., Couchman H. M. P., 1992, MNRAS, 257, 11

van den Bosch F. C., 2001, MNRAS, 327, 1334

van den Bosch F. C., Abel T., Croft R. A. C., Hernquist L., White S. D. M., 2002, ApJ, in press

van den Bosch F. C., Burkert A., Swaters R. A., 2001, MNRAS, 326, 1205

Wada K., 2001, ApJ, 559, L41

Wada K., Norman C. A., 1999, ApJ, 516, L13

Walker I. R., Mihos J. C., Hernquist L., 1996, ApJ, 460, 121

Weinberg D. H., Hernquist L., Katz N., 1997, ApJ, 477, 8

Weinberg D. H., Hernquist L., Katz N., 2002, ApJ, 571, 15

White M., Hernquist L., Springel V., 2002, preprint, astro-ph/0205437

White S. D. M., Frenk C. S., 1991, ApJ, 379, 52

White S. D. M., Rees M. J., 1978, MNRAS, 183, 341

Yepes G., Kates R., Khokhlov A., Klypin A., 1997, MNRAS, 284, 235

Zhang Y., Anninos P., Norman M. L., 1995, ApJ, 453, L57